Atmos. Chem. Phys., 12, 10367–10385, 2012
www.atmos-chem-phys.net/12/10367/2012/
doi:10.5194/acp-12-10367-2012

Atmospheric Chemistry and Physics

FTIR time-series of biomass burning products (HCN, C_2H_6, C_2H_2, CH_3OH, and HCOOH) at Reunion Island (21° S, 55° E) and comparisons with model data

C. Vigouroux[1], T. Stavrakou[1], C. Whaley[2], B. Dils[1], V. Duflot[3,*], C. Hermans[1], N. Kumps[1], J.-M. Metzger[3], F. Scolas[1], G. Vanhaelewyn[1,], J.-F. Müller[1], D. B. A. Jones[2], Q. Li[4], and M. De Mazière[1]**

[1]Belgian Institute for Space Aeronomy (BIRA-IASB), Brussels, Belgium
[2]Department of Physics, University of Toronto, Canada
[3]Laboratoire de l'Atmosphère et des Cyclones (LACy), Université de La Réunion, France
[4]LAGEO, Institute of Atmospheric Physics, Chinese Academy of Sciences, China
[*]now at: the Laboratory of Quantic Chemistry and Photophysics, Université Libre de Bruxelles, Belgium
[**]now at: Department of Solid State Sciences, Ghent University, Belgium

Correspondence to: C. Vigouroux (corinne.vigouroux@aeronomie.be)

Received: 26 March 2012 – Published in Atmos. Chem. Phys. Discuss.: 4 June 2012
Revised: 23 October 2012 – Accepted: 30 October 2012 – Published: 7 November 2012

Abstract. Reunion Island (21° S, 55° E), situated in the Indian Ocean at about 800 km east of Madagascar, is appropriately located to monitor the outflow of biomass burning pollution from Southern Africa and Madagascar, in the case of short-lived compounds, and from other Southern Hemispheric landmasses such as South America, in the case of longer-lived species. Ground-based Fourier transform infrared (FTIR) solar absorption observations are sensitive to a large number of biomass burning products. We present in this work the FTIR retrieval strategies, suitable for very humid sites such as Reunion Island, for hydrogen cyanide (HCN), ethane (C_2H_6), acetylene (C_2H_2), methanol (CH_3OH), and formic acid (HCOOH). We provide their total columns time-series obtained from the measurements during August–October 2004, May–October 2007, and May 2009–December 2010. We show that biomass burning explains a large part of the observed seasonal and interannual variability of the chemical species. The correlations between the daily mean total columns of each of the species and those of CO, also measured with our FTIR spectrometer at Reunion Island, are very good from August to November ($R \geq 0.86$). This allows us to derive, for that period, the following enhancement ratios with respect to CO: 0.0047, 0.0078, 0.0020, 0.012, and 0.0046 for HCN, C_2H_6, C_2H_2, CH_3OH, and HCOOH, respectively. The HCN ground-based data are compared to the chemical transport model GEOS-Chem, while the data for the other species are compared to the IMAGESv2 model. We show that using the HCN/CO ratio derived from our measurements (0.0047) in GEOS-Chem reduces the underestimation of the modeled HCN columns compared with the FTIR measurements. The comparisons between IMAGESv2 and the long-lived species C_2H_6 and C_2H_2 indicate that the biomass burning emissions used in the model (from the GFED3 inventory) are probably underestimated in the late September–October period for all years of measurements, and especially in 2004. The comparisons with the short-lived species, CH_3OH and HCOOH, with lifetimes of around 5 days, suggest that the emission underestimation in late September–October 2004, occurs more specifically in the Southeastern Africa-Madagascar region. The very good correlation of CH_3OH and HCOOH with CO suggests that, despite the dominance of the biogenic source of these compounds on the global scale, biomass burning is their major source at Reunion Island between August and November.

Published by Copernicus Publications on behalf of the European Geosciences Union.

1 Introduction

Biomass burning is a major source for many atmospheric pollutants released in the atmosphere (Crutzen and Andreae, 1990), especially in the Tropics with a dominant contribution of savanna fires (Andreae and Merlet, 2001; Akagi et al., 2011). Reunion Island (21° S, 55° E), situated in the Indian Ocean at about 800 km east of Madagascar is appropriately located to monitor the biomass burning pollution outflow from Madagascar (Vigouroux et al., 2009), Southern Africa (Randriambelo et al., 2000), and even South America in the case of long-lived species such as CO (Duflot et al., 2010). We have used ground-based FTIR measurements from August to October 2004, May to October 2007, and May 2009 to December 2010 to derive time-series of total columns of five trace gases produced by vegetation fires: hydrogen cyanide (HCN), ethane (C_2H_6), acetylene (C_2H_2), methanol (CH_3OH), and formic acid (HCOOH). Considering their long lifetime, hydrogen cyanide (about 5 months in the troposphere, Li et al., 2003), ethane (80 days, Xiao et al., 2008) and acetylene (2 weeks, Xiao et al., 2007) are well-known tracers for the transport of tropospheric pollution, and have already been measured by ground-based FTIR technique at several locations in the Northern Hemisphere (Mahieu et al., 1997; Rinsland et al., 1999; Zhao et al., 2002) and in the Southern Hemisphere, namely in Lauder (New Zealand) at 45° S (Rinsland et al., 2002), in Wollongong (Australia) at 34° S (Rinsland et al., 2001), and in Darwin (Australia) at 12° S (Paton-Walsh et al., 2010). Reunion Island is the only FTIR site located sufficiently close to Southern Africa and Madagascar that it can monitor the outflow of shorter-lived species emitted in these regions. Methanol and formic acid are such shorter-lived species with global lifetimes of 6 days (Stavrakou et al., 2011) and 3–4 days (Paulot et al., 2011; Stavrakou et al., 2012), respectively. Although these species are predominantly biogenic in a global scale (Jacob et al., 2005; Millet et al., 2008; Stavrakou et al., 2011; Paulot et al., 2011; Stavrakou et al., 2012), we show that pyrogenic contributions are important during the more intense biomass burning period at Reunion Island. Only a few ground-based FTIR studies have focused on these two species: methanol has been measured in Wollongong (Paton-Walsh et al., 2008) and Kitt Peak, 32° N (Rinsland et al., 2009), and formic acid mainly in the Northern Hemisphere (Rinsland et al., 2004; Zander et al., 2010; Paulot et al., 2011), but also in Wollongong (Paulot et al., 2011).

Because of its location, Reunion Island is very well situated to evaluate the emission and transport of various biogenic and pyrogenic species in chemical transport models. Previous comparisons of our FTIR measurements of formaldehyde during the 2004 and 2007 campaigns with IMAGES model simulations (Müller and Brasseur, 1995) have shown an overall good agreement, but also suggested that the emissions of formaldehyde precursors at Madagascar might be underestimated by the model (Vigouroux et al., 2009). Our FTIR measurements of methanol and formic acid at Reunion Island in 2009 were already used to validate an inverse modeling approach of IASI data, which resulted in improved global emission budgets for these species (Stavrakou et al., 2011, 2012, respectively). Also Paulot et al. (2011) used our total column data of formic acid for 2009 for comparison with the GEOS-Chem model. However, in these three studies, the FTIR data were described only briefly. Therefore, a complete description of these methanol and formic acid data is given here, including the retrieval strategies and data characterization. At the same time, we present the more recently retrieved species HCN, C_2H_6, and C_2H_2. For all these species except HCN, we show comparisons of their daily mean total columns with corresponding IMAGES simulations, for the individual campaigns from 2004 to December 2010. Because IMAGES does not calculate HCN, we compare its daily mean total columns to GEOS-Chem simulations, for the years 2004 and 2007.

To quantify the atmospheric impact of biomass burning in the chemical transport models, the emission factors of the pyrogenic species have to be implemented accurately. As these emission factors depend not only on the species but also on the type of fire and even on the specific conditions prevailing at each fire event, many different values have been reported, for various gases at various locations in the world. Compilations of these numerous data are published regularly in order to facilitate their use by the modeling community (Andreae and Merlet, 2001; Akagi et al., 2011). A common way of deriving an emission factor is the measurement of the emission ratio of the target species relative to a reference species, which is often CO_2 or CO. When the measurement occurs in an aged plume, this same ratio is called "enhancement ratio" by opposition to the emission ratio measured at the source of the fire. These enhancement ratios can be used to interpret the ongoing chemistry within the plume. Recently, there has been an interest in deriving such enhancement ratios from satellite data in the Northern Hemisphere (Rinsland et al., 2007; Coheur et al., 2009) and in the Southern Hemisphere (Rinsland et al., 2006; Dufour et al., 2006; González Abad et al., 2009), or both (Tereszchuk et al., 2011). For weakly reactive species, the enhancement ratio should be similar to the emission ratio, as long as the compound is not photochemically produced from the degradation of other pyrogenic NMVOCs. We use our FTIR measurements of CO total columns at Reunion Island (Duflot et al., 2010) to show that during the August–November period the correlation between all the species and CO is very good ($R \geq 0.86$), suggesting that the common predominant source is biomass burning. We can then derive enhancement ratios of HCN, C_2H_6, C_2H_2, CH_3OH, and HCOOH from the regression slope of their total column abundance versus that of CO. Considering the relatively long lifetime of these species (5 months to 4 days), we can compare them to emission ratios found in the literature.

Section 2 gives a description of the retrieval strategies optimized for each species, the main difficulties being the weak

absorption signatures of the target gases, especially relative to the strong interference with water vapour lines, in the very humid site of Saint-Denis, Reunion Island. All species are characterized by their averaging kernels and their error budget. The seasonal and interannual variability of the species is discussed in Sect. 3. The correlation with CO and the enhancement ratios relative to CO are then given and compared to literature values in Sect. 4. Finally, we show and discuss the model comparisons in Sect. 5.

2 FTIR data: description and charaterization

2.1 Measurements campaigns

A Bruker 120M Fourier transform infrared (FTIR) spectrometer has been deployed during three campaigns at Saint-Denis in Reunion Island (21° S, 55° E, altitude 50 m), in October 2002, from August to October 2004, and from May to November 2007, and for continuous observations starting in May 2009. The total spectral domain covered by our FTIR solar absorption measurements is 600 to 4500 cm^{-1} but, depending on the species, specific bandpass filters and detectors are used (see Senten et al. (2008) for details). The spectrometer was operated in an automatic and remotely controlled way by use of BARCOS (Bruker Automation and Remote COntrol System) developed at BIRA-IASB (Neefs et al., 2007). More detailed specifications of the 2002 and 2004 experiments are given in Senten et al. (2008). The later experiments are conducted in an almost identical way. In the present work, we will focus on the 2004, 2007, and 2009–2010 time-series.

The volume mixing ratio profiles of target gases are retrieved from the shapes of their absorption lines, which are pressure and temperature dependent. Daily pressure and temperature profiles have been taken from the National Centers for Environmental Prediction (NCEP). The observed absorption line shapes also depend on the instrument line shape (ILS) which is therefore included in the forward model of the retrieval code. In order to characterize the ILS and to verify the alignment of the instrument, a reference low-pressure (2 hPa) HBr cell spectrum is recorded at local noon with the sun as light source, whenever the meteorological conditions allow so, but also each evening using a lamp as light source. The software LINEFIT is used for the analysis of the cell spectra, as described in Hase et al. (1999). In this approach, the complex modulation efficiencies are described by 40 parameters (20 for amplitude and 20 for phase orientation) at equidistant optical path differences.

2.2 Retrieval strategies

The FTIR retrievals are performed using the algorithm SFIT2 (Rinsland et al., 1998), version 3.94, jointly developed at the NASA Langley Research Center, the National Center for Atmospheric Research (NCAR) and the National Institute of Water and Atmosphere Research (NIWA). The spectral inversion is based on a semi-empirical implementation of the Optimal Estimation Method (OEM) of Rodgers (2000), which implies the use of an a priori information (a priori profiles and regularization matrix **R**). The retrieved vertical profiles are obtained by fitting one or more narrow spectral intervals (microwindows).

2.2.1 Choice of microwindows and spectroscopic databases

We have used, for all species except C_2H_6, the HITRAN 2008 spectroscopic line parameters (Rothman et al., 2009). For C_2H_6, we used the pseudo-lines constructed by G. Toon (personal communication, 2010, see http://mark4sun.jpl.nasa.gov/pseudo.html for details), based on the recent paper of Harrison et al. (2010).

Table 1 gives the list of microwindows used in this work. All target species have weak absorptions in the infrared. It is therefore important to choose the spectral microwindows in order to minimize the impact of interfering species. The particular difficulty at Saint-Denis is the presence of very strong absorption lines of water vapour in the spectra, in most spectral regions. As can be seen in the table, it is impossible to select spectral regions without interferences of $H_2{}^{16}O$ and/or of isotopologues. In the retrieval process, while a vertical profile is fitted for the target species, a single scaling of their a priori profile is done for the interfering species. For the interfering species having a small impact on the retrievals, a single climatological a priori profile is used for all spectra. For the other ones, such as water vapour, we performed beforehand and independently profile retrievals in dedicated microwindows for each spectrum. These individual retrieved profiles were then used as the a priori profiles in the retrievals of the target species; they are again fitted, but now with only one scaling parameter.

For the retrieval of HCN, we followed the approach of Paton-Walsh et al. (2010) perfectly adapted for humid sites such as Saint-Denis. For humid sites (i.e., tropical sites at low altitude), we do not recommend any of the commonly used micro-windows sets comprising the 3287.248 cm^{-1} line (Mahieu et al., 1997; Rinsland et al., 1999; Notholt et al., 2000; Rinsland et al., 2001, 2002; Zhao et al., 2002). Preliminary retrievals of $H_2{}^{16}O$, $H_2{}^{18}O$ and $H_2{}^{17}O$ were made independently in the 3189.50–3190.45 cm^{-1}, 3299.0–3299.6 cm^{-1}, and 3249.7–3250.3 cm^{-1} spectral intervals, respectively. The $H_2{}^{16}O$ and $H_2{}^{18}O$ retrieval results are also used as a priori profiles for the C_2H_2 retrievals.

For C_2H_6, the widely used (Mahieu et al., 1997; Notholt et al., 2000; Rinsland et al., 2002; Zhao et al., 2002; Paton-Walsh et al., 2010) microwindow around 2976.8 cm^{-1} has been fitted together with one of the two other regions suggested in Meier et al. (2004), around 2983.3 cm^{-1}, in order to increase the DOFS. We decided to skip the other one, around 2986.7 cm^{-1}, also used in Notholt et al. (1997), because of the very strong $H_2{}^{16}O$ line nearby. Independent beforehand

Table 1. Microwindows (in cm^{-1}) and interfering species used for the retrievals of HCN, C_2H_6, C_2H_2, HCOOH, and CH_3OH.

Target gas	Microwindows (cm^{-1})	Interfering species
HCN	3268.05–3268.35	H_2O, $H_2{}^{18}O$, $H_2{}^{17}O$
	3331.40–3331.80	H_2O, $H_2{}^{17}O$, CO_2, N_2O solar CO
C_2H_6	2976.66–2976.95	H_2O, $H_2{}^{18}O$, O_3
	2983.20–2983.55	H_2O, $H_2{}^{18}O$, O_3
C_2H_2	3250.25–3251.11	H_2O, $H_2{}^{18}O$, solar CO
CH_3OH	1029.00–1037.00	H_2O, O_3, $^{16}O^{16}O^{18}O$, $^{16}O^{18}O^{16}O$, $^{16}O^{16}O^{17}O$, $^{16}O^{17}O^{16}O$, CO_2, NH_3
HCOOH	1102.75–1106.40	HDO, H_2O, $H_2{}^{18}O$, $H_2^{17}O$, O_3, $^{16}O^{16}O^{18}O$, NH_3 CCl_2F_2, CHF_2Cl, CH_4

retrievals of $H_2{}^{16}O$ were made in the 2924.10–2924.32 cm^{-1} microwindow. Because of the lower influence of $H_2{}^{18}O$ and the difficulty of finding an isolated $H_2{}^{18}O$ line in this spectral region, we simply used the individual retrieved $H_2{}^{16}O$ profiles also as the a priori for $H_2{}^{18}O$. Ozone is a minor interfering species here, we therefore used a single a priori profile for all the spectra, calculated at Reunion Island (J. Hannigan, NCAR, personal communication, 2010) from the Whole Atmosphere Community Climate Model (WACCM [1], version 5).

For C_2H_2, we have chosen the line at 3250.66 cm^{-1} following Notholt et al. (2000); Rinsland et al. (2002); Zhao et al. (2002). The other lines suggested in Meier et al. (2004), of which some are used in Notholt et al. (1997); Paton-Walsh et al. (2010), have been tested but gave poorer results. For the CO solar lines, we used the empirical line-by-line model of Hase et al. (2006); the linelist was updated according to Hase et al. (2010).

For HCOOH, we used the Q-branch of the ν_6 mode, as in other retrievals of satellite (González Abad et al., 2009; Razavi et al., 2011) or ground-based (Rinsland et al., 2004; Zander et al., 2010) infrared measurements. The main difficulty is the HDO absorption overlapping the HCOOH Q-branch. We have therefore performed preliminary retrievals of HDO in the 1208.49–1209.07 cm^{-1} microwindow, for each spectrum. $CHClF_2$ and CCl_2F_2 profiles were also retrieved independently in the 828.62–829.35 cm^{-1} and 1160.2–1161.4 cm^{-1} spectral intervals, respectively. The O_3 vertical profiles were also retrieved beforehand using the optimized strategy described in Vigouroux et al. (2008) for the same spectra (microwindow 1000–1005 cm^{-1}). These profiles are used as individual a priori profiles, in the retrieval of HCOOH, not only for O_3 but also for its isotopologues. Finally, $H_2{}^{16}O$ was retrieved beforehand in the 834.6–836.6 cm^{-1} microwindow, and the resulting profiles were used as a priori for all water vapour isotopologues (except HDO). Unique a priori profiles were used for CH_4 (from WACCMv5) and NH_3.

CH_3OH has been studied in ground-based infrared measurements only recently (Paton-Walsh et al., 2008; Rinsland et al., 2009), with different choices of microwindows, both around 10 µm. In the case of Saint-Denis, the best sensitivity to CH_3OH is obtained by using the Q-branch of the ν_8 mode at about 1033 cm^{-1}, as in Paton-Walsh et al. (2008). The same H_2O and O_3 individual a priori profiles as for HCOOH are used in the methanol retrievals. Unique a priori profiles were used for CO_2 (from WACCMv5) and NH_3.

2.2.2 Choice of a priori profiles and regularization

The a priori profiles adopted in the FTIR retrievals of the target species are shown in Fig. 1.

The HCN a priori profile is the mean of the HCN profiles, calculated at Reunion Island (J. Hannigan, personal communication, 2010) from WACCMv5 from 2004 to 2006. The CH_3OH a priori profile, from the ground to 12 km, is a smoothed approximation of data composites of the airborne experiment PEM-Tropics-B (Raper et al., 2001), as was done for HCHO in Vigouroux et al. (2009): we used the average concentration over the Southern tropical Pacific (0 to 30° S; 160° E to 95° W) based on the data composites available at http://acd.ucar.edu/~emmons/DATACOMP/camp_table.htm, which provides an update of the database described in Emmons et al. (2000). The HCOOH a priori profile, from the ground to 7 km, has been constructed from the data composites of the airborne experiment PEM-Tropics-A (Hoell et al., 1999) also available at the previous link, and from ACE-FTS satellite measurements above Reunion Island for the 7–30 km range (González Abad, personal communication, 2010; see González Abad et al., 2009). For C_2H_6, from the ground to 12 km, we used the mean of PEM-Tropics-B and PEM-Tropics-A measurements. For C_2H_2, since the mean of PEM-Tropics-B and PEM-Tropics-A measurements at 7 km was almost two times lower than the value measured by ACE-FTS above Reunion Island (N. Allen, personal communication, 2010), we took the mean of both measurement values at this altitude and used this same value down to the ground; above, we used the ACE measurements but scaled to the value at 7 km. For altitudes above which no information was available, we have decreased the vmr values smoothly to zero.

In the usual OEM, the constraint matrix $\mathbf{R}$ is the inverse of the a priori covariance matrix $\mathbf{S}_a$. Ideally, $\mathbf{S}_a$ should express the natural variability of the target gas, and thus should be as realistic as possible and evaluated from appropriate

[1] http://www.cesm.ucar.edu/working_groups/WACCM/

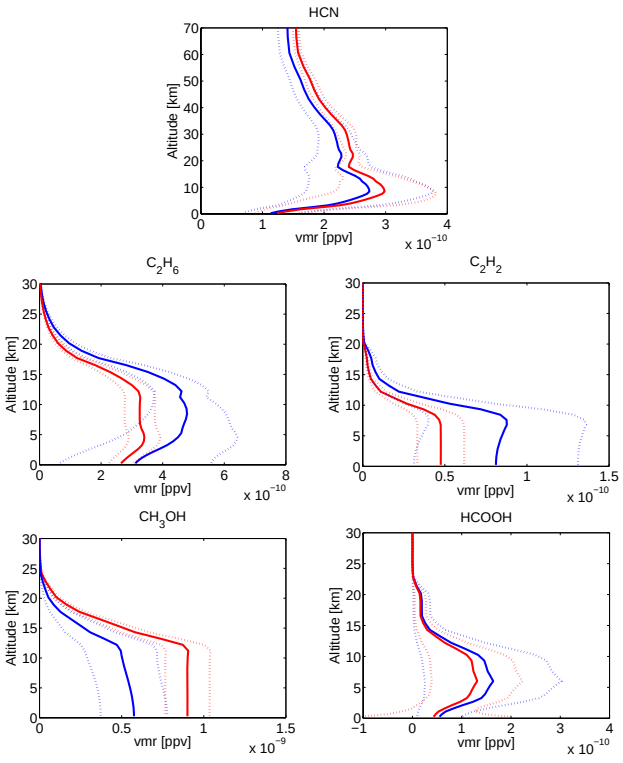

Fig. 1. A priori vertical profiles (red lines; Sect. 2.2.2) and variability used for smoothing error calculation (red dashed lines; Sect. 2.3) of the five retrieved species (in vmr, ppv). The HCN a priori profile is given by the WACCM, v5 model. The a priori profiles of the other species have been constructed using a combination of airborne and ACE-FTS measurements (see text for details). The means (blue lines) and standard deviations (blue dashed lines) of the retrieved FTIR profiles over the whole dataset are also shown for comparison.

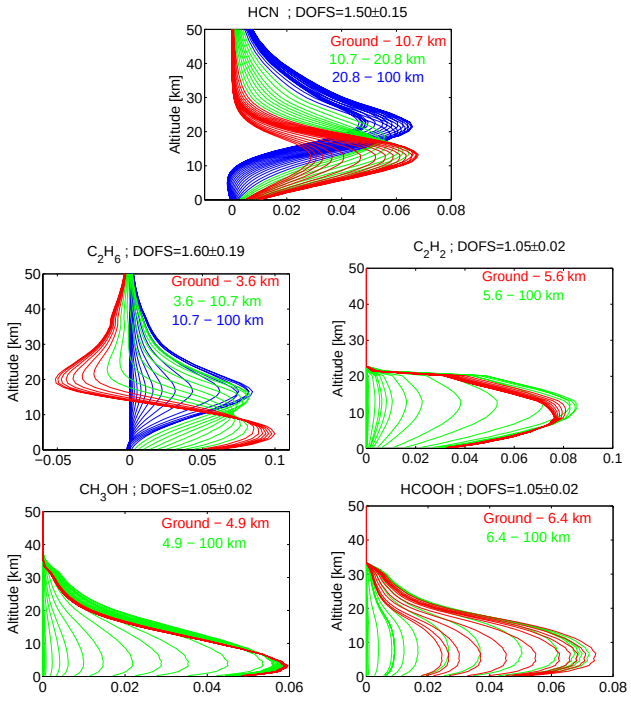

Fig. 2. FTIR volume mixing ratio averaging kernels (ppv ppv^{-1}) of the five retrieved species. The total DOFS for each species is given in the titles. Each line corresponds to the averaging kernel at a given altitude, the retrievals being made with a 47 layers grid. We have used the same color for the averaging kernels at altitudes lying in a partial column for which we have about a DOFS of 0.5. The partial columns boundaries are given in the legends.

climatological data (Rodgers, 2000). However, for our target species at Reunion Island, this information is poorly available and therefore we have opted for Tikhonov L_1 regularization (Tikhonov, 1963) as in Vigouroux et al. (2009), i.e., the constraint matrix is defined as $\mathbf{R} = \alpha \mathbf{L_1^T L_1}$, with α the regularization strength and $\mathbf{L_1}$ the first derivative operator. For determining the strength of the constraint (α), we have followed the method illustrated in Fig. 4 of Steck (2002): we have chosen, for each target species, the parameter α that minimizes the total error (measurement noise + smoothing error).

The vertical information contained in the FTIR retrievals are characterized by the averaging kernel matrix **A** and its trace gives the degrees of freedom for signal (DOFS). We obtain mean DOFS of about 1.50 ± 0.15 for HCN, 1.60 ± 0.19 for C_2H_6, and 1.05 ± 0.02 for C_2H_2, HCOOH and CH_3OH. We therefore use only total column results in our comparisons with the model. It is worth noticing that the total column results shown in this paper are representative of the tropospheric columns of the species, since the cold-point tropopause lies around 17 km at Reunion Island (Sivakumar et al., 2006) and the partial columns from the ground up to 17 km represent more than 98 % of the total column amounts for all species, except HCN (91 %).

The means of the averaging kernels (rows of **A**) for each molecule are shown in Fig. 2. As expected with DOFS close to one (except for C_2H_6 and HCN), we can see that the averaging kernels are not vertically resolved. For each species, they all peak at about the same altitude (around 10 km for C_2H_2; 5 km for HCOOH; and 3 km for CH_3OH). For C_2H_6 and HCN, we obtain two maxima: at about 5 and 15 km, and at about 13 and 21 km, respectively. Since we discuss total column results, we also show in Fig. 3 the total column averaging kernel for each species.

2.3 FTIR error budget

The error budget is calculated following the formalism of Rodgers (2000), and can be divided into three different error sources: the smoothing error expressing the uncertainty due to the limited vertical resolution of the retrieval, the forward model parameters error, and the measurement noise error.

The smoothing error covariance is calculated as $(\mathbf{I}-\mathbf{A})\mathbf{S}_{\mathrm{var}}(\mathbf{I}-\mathbf{A})^T$, where $\mathbf{S}_{\mathrm{var}}$ is the best possible estimate of the

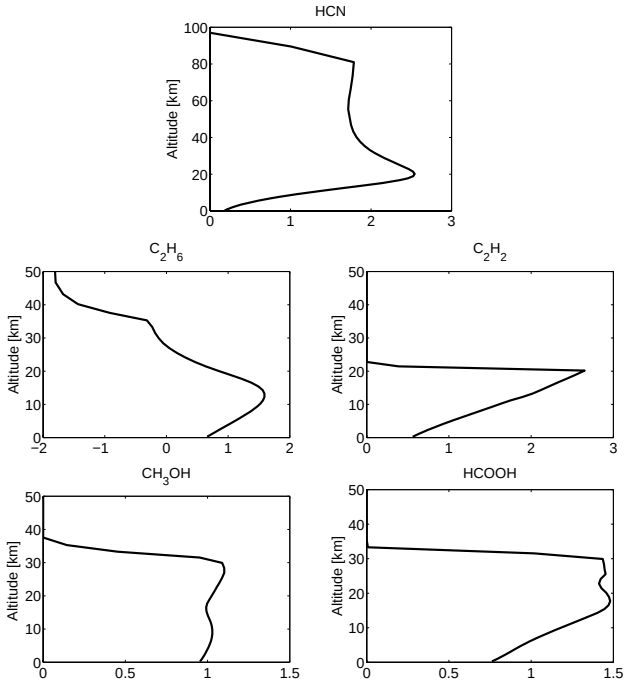

Fig. 3. FTIR total column averaging kernels (molec cm^{-2}/molec cm^{-2}) of the five retrieved species.

natural variability of the target molecule. For HCN, we use the full covariance matrix constructed with the same modeled profiles from WACCMv5 as for the HCN a priori profile. The vertical resolution of the WACCMv5 model used in this work is less than 1 km below 13 km, and less than 1 km below 30 km. The diagonal elements of the covariance matrix correspond to a variability of about 30 % at the ground increasing up to 40 % at 3 km, and then decreasing rapidly (24 % at 10 km and 5 % at 20 km and above). The off-diagonal elements correspond approximately to a Gaussian correlation with a correlation length of 6 km. For the other species, the diagonal elements of $\mathbf{S}_{\text{var}}$ are estimated from the average observed variability in $5^\circ \times 5^\circ$ pixels during PEM-Tropics-B and PEM-Tropics-A. The vertical resolution of these aircraft data is 1 km. For C_2H_6 and C_2H_2, approximately constant values of 15 % and 30 % are observed, respectively, at all altitudes up to 12 km. For HCOOH, the variability decreases rapidly from 350 % at the surface to about 70 % at 2.5 km up to 12 km. For CH_3OH, the observed variability seems unrealistic (below 1 % at the surface up to only 2 % at 12 km), but the number of measurements for this species is much smaller. We have therefore decided to use a constant 15 % value as for C_2H_6, since the standard deviations observed by our FTIR measurements are similar for both species. For the latter four species, the off-diagonal elements of $\mathbf{S}_{\text{var}}$ are estimated using a Gaussian correlation between the layers, with a correlation length of 4 km. Our smoothing error estimation is based on our best current knowledge of the variability of the species, calculated here with respect to the vertical resolution of WACCMv5 (for HCN) and of aircraft data (for the other species), but it should be corrected once this knowledge will be improved. We see from Fig. 1, that the variability obtained by our FTIR measurements (blue dashed lines) is larger than the one we assumed for the smoothing error calculation, for all species but especially for C_2H_2. So our smoothing error budget given in Table 2 might be underestimated.

Table 2. Mean error budget on individual total columns. The mean standard deviations (SD) of daily means, for the days when the number of measurements were equal or greater than three, are also given. The total error includes the smoothing error.

Errors (in %)	HCN	C_2H_6	C_2H_2	CH_3OH	HCOOH
Smoothing	9	2	3	0.3	7
Random	2	5	16	10	11
SD	3	6	14	8	15
Systematic	14	5	7	9	15
Total error	17	7	17	13	19

All the details on the calculation of the measurement noise error and the forward model parameters error can be found in Vigouroux et al. (2009). The only difference concerns the error due to interfering species: in the present work, the $\mathbf{S}_{\text{b}}$ matrix (covariance matrix of the vector of model paremeters) has been constructed according to a constant (vs altitude) variability of 10 % and a Gaussian correlation between the layers with a 3 km correlation length.

The largest contributions to the model parameters random error are due to the temperature, the interfering species and the ILS uncertainties. The model parameters giving rise to a systematic error are the spectroscopic parameters: the line intensities and the pressure broadening coefficients of the absorption lines present in our micro-windows.

Table 2 summarizes, for the total columns of each species, the smoothing error, the total random and the total systematic error budget. The dominant contribution to the random error is, for each species, the random noise, except for methanol for which the temperature error contribution is the largest. We give also in Table 2 the mean of the standard deviations of each daily means for the days when the number of measurements were equal or greater than three. As we do not expect our target species total columns to vary much during the day, these standard deviation values give an estimation of the random error made on an individual total column retrieval. Indeed, the standard deviations are in good agreement with the total random errors given in the table.

3 FTIR time-series: seasonality and interannual variability

The time-series of the FTIR daily means total columns of HCN, C_2H_6, C_2H_2, CH_3OH, and HCOOH are shown in Fig. 4 (blue circles). In addition, we show the CO time-series, also measured with our FTIR spectrometer at Reunion Island (see Duflot et al. (2010) for details on the CO retrievals), because we discuss the correlation between CO and the five target species in the next section. The number of measurements within a day varies from 1 to 20, but with a median value of only 2. The smoothing error is not included in the error bars shown in Fig. 4 since we will discuss in Sect. 5 the comparisons with the model data that have been smoothed by the FTIR averaging kernels.

First, we observe maximum total column amounts in October for all species, as we already found for CO (Duflot et al., 2010), and as was observed also for ozone from radiosoundings (Randriambelo et al., 2000) at Reunion Island. It has been estimated that the biomass burning emission peak occurs in September in the Southern Hemisphere as a whole (Duncan et al., 2003). This is illustrated in Fig. 5 (top panel), where we show the CO emissions from the Global Fire Emission Database GFED2 and GFED3 for the whole Southern Hemisphere. However, there are important seasonal differences between different regions, depending on the timing of the dry season (Cooke et al., 1996). While the peak occurs generally in September in Southern Africa, the east coast (Mozambique) shows strong emissions also in October and to a lesser extent in November (Duncan et al., 2003). At Madagascar, the peak of the biomass burning emissions occurs in October (Cooke et al., 1996; Randriambelo et al., 1998). The latter two studies noted a peak fire displacement from the west coast of Madagascar in August (savanna), to the east coast in October (rain forest). The strong emissions in the eastern part of Southern Africa and Madagascar explain the peak in October observed for the species with a short lifetime (6 and 4 days for methanol and formic acid, respectively), while for the long-lived species HCN and C_2H_6 (5 and 2 months lifetime, respectively), the accumulation due to the September peak in South America (Duncan et al., 2003) and global Southern Africa also plays a role.

Concerning the interannual variability, the annual carbon emission estimates over 1997–2009 (Table 7 of van der Werf et al., 2010) show a high variability in South America (1-σ standard deviation of 51 %), and a low variability in Southern Africa (1-$\sigma = 10$ %). The interannual variability of CO emissions in the Southern Hemisphere, shown in Fig. 5 (top panel), is therefore mainly due to the South American tropical forest fires. The low variability of Southern Africa emissions is illustrated in Fig. 5 (middle panel). Table 7 of van der Werf et al. (2010), updated for the year 2010[2], shows annual carbon emissions that are 9 % and 3 % above the 1997–2010 mean values for South America and Southern Africa, respectively, in 2004; and 91 % above and 5 % below, respectively, in 2007. In 2009, they are 70 % and 3 % below the 1997–2010 mean values for South America and Southern Africa, respectively; and in 2010, 125 % and 10 % above, respectively. It has been shown that biomass burning from South America yields an important contribution to the CO columns above Reunion Island in 2007, especially in September and October (Fig. 15 of Duflot et al., 2010). Since ethane has a similar lifetime as CO, and HCN an even longer one, one expects to observe larger values of the two species amounts in September and October 2007 compared to 2004 and 2009. This is indeed the case, as can be observed in Fig. 4: larger values are obtained in October 2007 compared to October 2004, and in September 2007 compared to September 2009. The lack of data in October 2009 does not allow conclusion for this month. Larger values are observed in December 2010 compared to December 2009 for these two species. We can therefore conclude that the interannual variability of biomass burning emissions in the Southern Hemisphere is well observed at Reunion Island in the C_2H_6 and HCN total column amounts. However, if an interannual variability is indeed observed, its amplitude is well below the variability observed in the fire emission estimates in South America, suggesting that the influence of South American fires is present but is diluted at Reunion Island, possibly partly hidden by higher contributions from nearer fires.

On the contrary, we do not observe significant interannual differences for methanol and formic acid. Although biomass burning emissions are only a small source of methanol and formic acid, even in the Southern Hemisphere, when annual means are concerned (Sect. 5.1.2), they represent a significant contribution in the August-October period. To illustrate this, the model simulations obtained when the biomass burning contribution is removed is plotted for the two species in Fig. 4 (black solid line when removed from the standard run; red solid line from the optimized run using IASI data in 2009). Due to the short lifetime of these two species, biomass burning emissions in South America have little influence on the total columns above Reunion Island. The low interannual variability observed in the FTIR total columns during this period therefore reflects the low variability of the biogenic and photochemical contributions to the total budget of these compounds (see Sect. 5.1.2) and the weak variability of biomass burning emissions in Southern Africa (1-$\sigma = 10$ % as seen above). However, these two species are highly sensitive to specific biomass burning events as shown by the presence of many outliers in their time-series, especially in October. To confirm that these extreme values are indeed related to biomass burning events, we show the correlation between the total columns of our target species and CO in the next section.

[2] at http://www.falw.vu/~gwerf/GFED/GFED3/tables/emis_C_absolute.txt

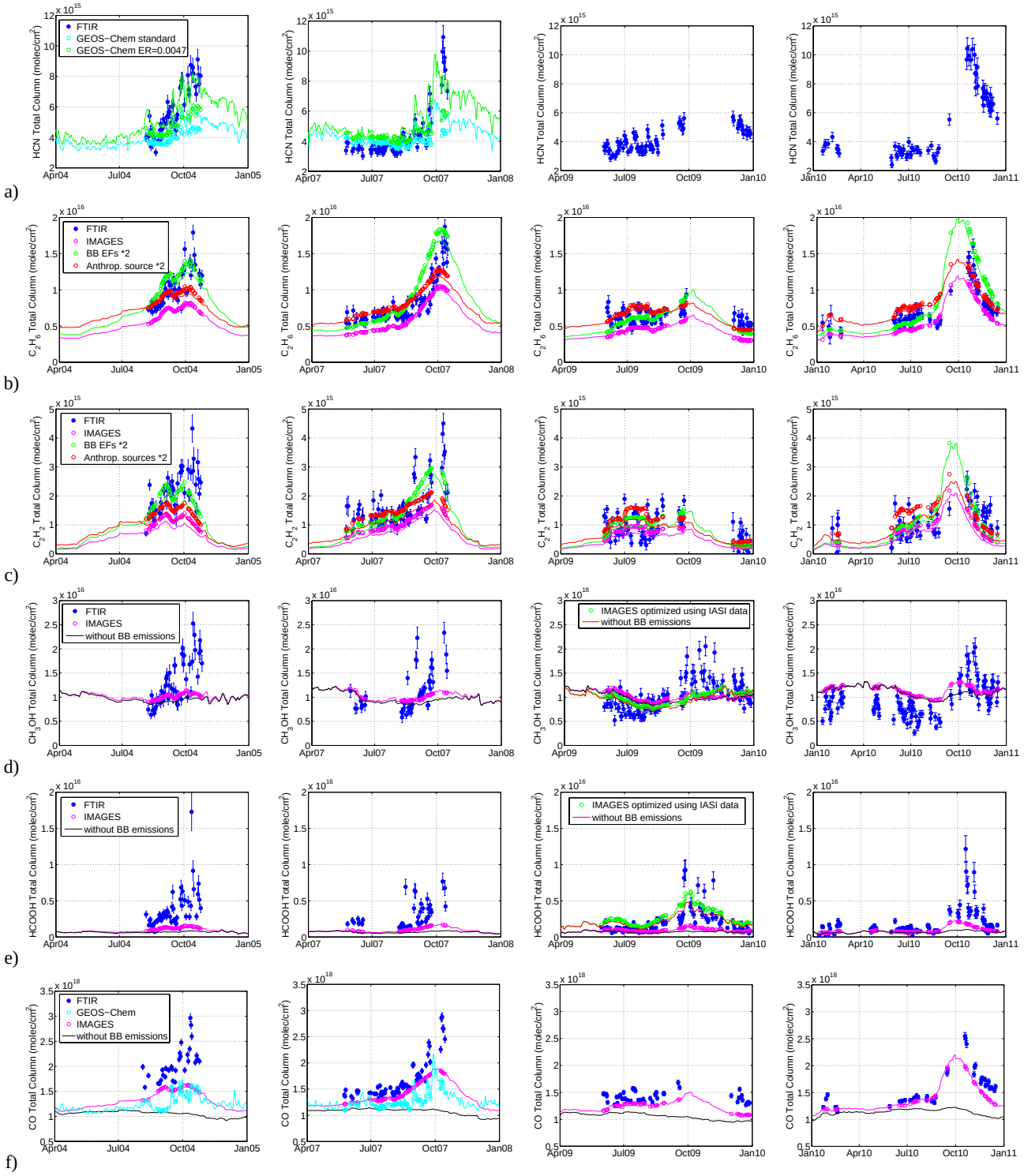

Fig. 4. Time-series of daily mean total columns at Reunion Island from: FTIR and GEOS-Chem HCN **(a)**, FTIR and IMAGES C_2H_6 **(b)**, C_2H_2 **(c)**, CH_3OH **(d)**, and HCOOH **(e)**. We also show the time-series of CO from Duflot et al. (2010), extended to 2009 and 2010 **(f)**. From left to right, the columns cover the years 2004, 2007, 2009, and 2010. The FTIR data are represented by the blue filled circles, different model simulations with the coloured lines (cyan and magenta for the standard runs of GEOS-Chem and IMAGEs, respectively; green and red for the sensitivity tests: see Sect. 5), and the model data smoothed with the FTIR averaging kernels with the open circles. For CH_3OH and HCOOH, the model simulations obtained when the biomass burning contribution is removed are shown in black for the standard run, and in red for the inversion using IASI data. (BB: biomass burning; ER: emission ratio; EF: emission factor; Anthrop.: anthropogenic).

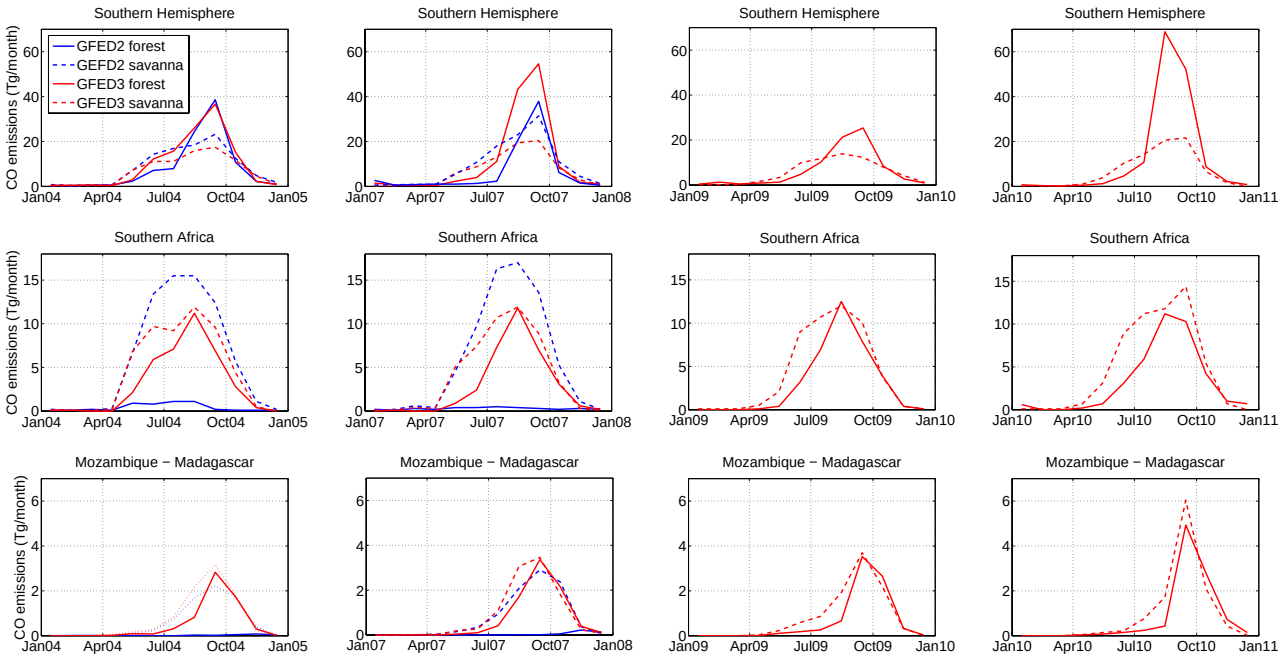

Fig. 5. CO emissions (Tg month^{-1}) from the GFED2 (in blue) and GFED3 (in red) inventories, for the southern Hemisphere (top panel), Southern Africa (middle panel), and the region of Mozambique and Madascar (bottom panel). The contribution from forests (solid lines) and savannas (dashed lines) are distinguished.

4 Correlation with CO and enhancement ratios

Figure 6 shows the correlation plots between the daily mean total columns of each of the five species discussed in this paper and those of CO (Duflot et al., 2010). We see from Fig. 6 that the correlation is very good ($R \geq 0.86$) for all species during the biomass burning period observed in Reunion Island (August–November, see previous section). This result indicates that CO and the five species share a common emission source, most probably biomass burning, which is responsible for most of their observed variability at Reunion Island during this period. Although the oxidation of methane and other organic compounds is a large source of CO, especially in the Tropics, its variability is low in comparison with vegetation fires, as reflected by the high correlation between CO and compounds such as HCN, C_2H_6 and C_2H_2, which are not produced photochemically in the atmosphere. Similarly, the biogenic source and the photochemical production of CH_3OH and HCOOH are unlikely to contribute significantly to the high correlation with CO.

The vertical columns sampled at Reunion Island represent a mix of airmasses with different ages since the time of emission. The highest columns are due to a predominance of fresh emissions in the sampled airmasses, and therefore to backward trajectories which were most often in the direct vicinity of emission regions in the previous days. Lower column values are more influenced by older emissions which might therefore originate in more distant areas. Distant fires (from e.g., South America) clearly cannot cause significant enhancements in CH_3OH and HCOOH (due to their short lifetimes). Their good correlation with CO confirms that those distant fires have a probably smaller impact on the variability of CO and other long-lived compounds than the nearby fires in Southern Africa and Madagascar. From backward trajectory simulations using FLEXPART, Duflot et al. (2010) concluded that the biomass burning emission contribution to the CO columns at Reunion Island from South America dominates the contribution of the Africa-Madagascar region in September–October 2007 (their Fig. 15). Our findings suggest however that, as far as short-term variability is concerned, Southern Africa and Madagascar fires have a major contribution at Reunion Island. This does not exclude a contribution of South American fires to the background levels of the long-lived pyrogenic compounds in the Southern Hemisphere, including Reunion Island, as suggested by the observed interannual variability of HCN and C_2H_6 (Sect. 3). It is noteworthy that there are large uncertainties residing in backward trajectory calculations, and also that the biomass burning emission inventory used in Duflot et al. (2010) (GFED2) could underestimate the emissions in the vicinity of Reunion Island (Southeastern Africa-Madagascar). Section 5 seems to confirm this conclusion.

We also evaluated the slope $\Delta X/\Delta CO$ for the measurements obtained during the August–November period for each species X. If we assume that, during this period, the excess total columns of X and CO are due to the biomass burning

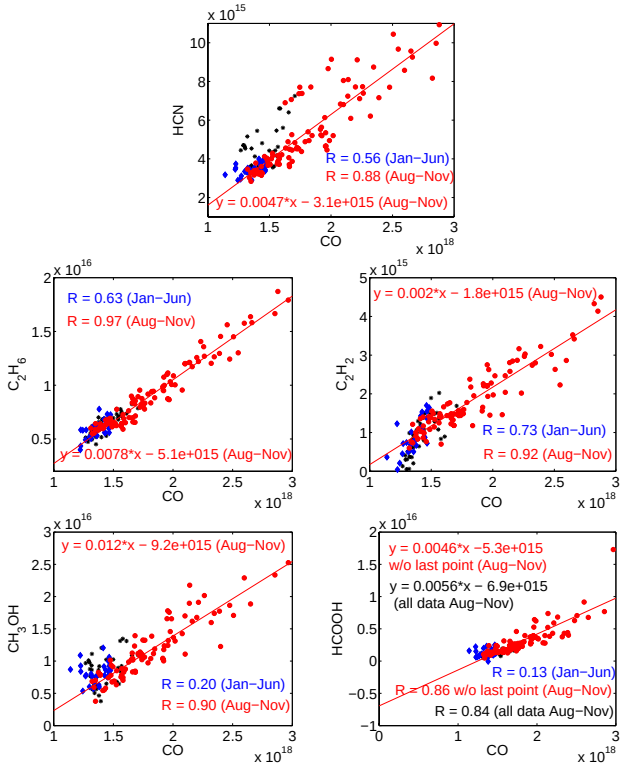

Fig. 6. Correlation plots of daily mean total columns of the five retrieved species versus CO (molec cm^{-2}). The correlation coefficient (R) is given for the periods from January to June (blue), and from August to November (red). For the latter period, the slope ($\Delta X/\Delta CO$) and the intercept from a linear least-squares fit of the data are also given.

events, then following Hornbrook et al. (2011) these slopes represent the "normalized excess mixing ratios" (also called the "enhancement ratios" as the plumes are far from the emission sources, as opposed to the emission ratios at the source, as defined in Andreae and Merlet, 2001). Given the relatively low reactivity and therefore long lifetimes of the species (from 5 months for HCN to 4 days for HCOOH), our "enhancement ratios" can be compared to the emission ratios (ER) obtained in previous studies. Indeed, from aircraft measurements of biomass burning plumes ranging from recent emissions to plumes aged of about one week, very little difference was observed between the emission ratio obtained at the source region and the enhancement ratios measured in plumes aged for methanol (Hornbrook et al., 2011). Also, the enhancement ratios of all our species measured by ACE-FTS in plumes aged of 5–6 days are very similar (and equal within the given standard deviations) to those obtained in plumes aged of 1–2 days (Table 2 in Tereszchuk et al., 2011).

Therefore, we compare in Table 3, the enhancement ratios obtained from our measurements between August and November, to emission ratios obtained from aircraft measurements of savanna fires in Southern Africa (Sinha et al., 2003), and to emission ratios derived from the latest compilation of emission factors (EF) by Akagi et al. (2011), for savanna and tropical forest. Following Andreae and Merlet (2001), we derive the "Akagi ER" from the equation:

$$\mathrm{ER}_{(\frac{X}{\mathrm{CO}})} = \frac{\mathrm{EF}_X}{\mathrm{EF}_{\mathrm{CO}}} \frac{\mathrm{MW}_{\mathrm{CO}}}{\mathrm{MW}_X},$$

where MW_X and $\mathrm{MW}_{\mathrm{CO}}$ are the molecular weights of the species X and the reference species CO in our case.

For the two long-lived species HCN and C_2H_6, our FTIR-derived enhancement ratios agree well with the compilation of Akagi et al. (2011), especially when the tropical forest values are considered. This could evidence for an influence of tropical forest fire emissions in South America to the observed concentrations of these long-lived species. But as noted previously and illustrated in Fig. 5 (bottom panel), the eastern part of Madagascar is also dominated by tropical forest, and woodland fires are also widespread in Mozambique/Zambia/Tanzania according to the GFED3 inventory (van der Werf et al., 2010). Moreover, the uncertainties on the emission factors given in Akagi et al. (2011) are quite large (40–60 % for HCN and C_2H_6), so this very good agreement should be interpreted with caution. For HCN, our enhancement ratio agrees very well with the value of 0.0047 ± 0.0005 obtained by Rinsland et al. (2002), using the same FTIR technique for the period July–September, at Lauder, New Zealand (45° S, 170° E). In the case of long-lived tracers, the emission ratios derived from the dry season measurements at Reunion Island reflect a mix of different vegetation types in the Southern Hemisphere, with however a strong influence of nearby regions (Madagascar and Southeastern Africa) as suggested by the good correlation between CH_3OH and HCOOH with CO. This kind of mixed emission (enhancement) ratios can be useful for models which do not include individual emission factors for different vegetation/fire types. This has been used in Sect. 5.2.1 when we compare FTIR HCN time-series with GEOS-Chem: replacing the HCN/CO ratio with our 0.0047 value significantly improved the agreement between data and model.

The enhancement ratio obtained for C_2H_2 (0.0020 ± 0.0001) does not agree with Sinha et al. (2003) nor with Akagi et al. (2011), but considering the 41 % and 80 % uncertainties in the emission factors given in Akagi et al. (2011) for savanna and tropical forest, respectively, we are still in the expected range of values. Indeed, one of the references used by Akagi et al. (2011) in the evaluation of the average emission factor for the tropical forest is the work of Ferek et al. (1998), who obtain a value of $0.0024(\pm 0.0004)$ from 19 airborne measurements in Brazil. Also Paton-Walsh et al. (2010) obtain an emission ratio of $0.0024(\pm 0.0003)$, from FTIR measurements of Australian savanna fire products, thus from a different vegetation type than Ferek et al. (1998). On the other hand, we obtain different values than Paton-Walsh et al. (2010) for HCN and C_2H_6.

Table 3. Enhancement ratios with respect to CO from this work. Also listed for comparison, the emission ratios with respect to CO from aircraft measurements over savanna fires in Southern Africa (Sinha et al., 2003), and derived from emission factors given in Akagi et al. (2011) (see text for details). The approximate tropospheric global lifetimes of each species are also given. The lifetime of CO is about 2 months (Xiao et al., 2007).

Species	Global lifetime	This work	Akagi et al. (2011) Tropical forest	Akagi et al. (2011) Savanna	Sinha et al. (2003) Savanna Southern Africa
HCN	5 months	0.0047 ± 0.0003	0.0047	0.0067	0.0085 ± 0.0029
C_2H_6	2 months	0.0078 ± 0.0002	0.0071	0.0098	0.0026 ± 0.0002
C_2H_2	2 weeks	0.0020 ± 0.0001	0.0051	0.0041	0.0043 ± 0.0013
CH_3OH	6 days	0.0116 ± 0.0006	0.0229	0.0164	0.015 ± 0.003
HCOOH	4 days	0.0046 ± 0.0003	0.0052	0.0020	0.0059 ± 0.0022

We see that the agreement is very good between our work and the measurements of savanna fires in Southern Africa (Sinha et al., 2003) for the two species with a shorter lifetime, formic acid and methanol. The agreement is also reasonable with the values of Akagi et al. (2011). Note that the HCOOH outlier at about 17×10^{15} molec cm^{-2} (Fig. 6) has been removed in the derivation of the enhancement ratio given in Table 3. This measurement is clearly seen in Fig. 4 in 2004 and corresponds to a day (12 October) where very high values are also observed in other species (C_2H_6, C_2H_2, HCHO in Vigouroux et al., 2009). The reason why this point is an outlier in the correlation plot, in contrast with the corresponding measurements for C_2H_6 and C_2H_2 is not clear at present, and may originate from the type of fire on that specific day. Trajectory calculations could possibly help to determine the origin of the airmass and possibly the fire type responsible for the observed enhancement.

However, the comparisons given in Table 3 and discussed above are only indicative, because we use all the measurements within the August–November period to derive the correlation plots, without making any distinction according to the origin of the different airmasses, i.e. forest or savanna. When the whole Southern Hemisphere is concerned, we see from Fig. 5 (top panel) that the peak of the emissions is dominated by the forest source. When considering Southern African emissions, we see an important difference between GFED2 and GFED3: the former includes almost no emission from the forest source, while for the latter the forest source is about as high as the savanna source (Fig. 5, middle and bottom panels). Trusting the GFED3 inventory, it is not possible to know, without precise quantitative backward trajectories, if our FTIR measurements are representative of forest or savanna emissions. Such backward trajectories analysis is beyond the scope of the paper. More insights will be obtained after additional years of measurements, in order to improve the statistics and to make a more quantitative study.

5 Comparisons with chemical transport models

5.1 Models description

5.1.1 HCN simulated in GEOS-Chem

GEOS-Chem (http://www.geos-chem.org/) is a global 3-D chemical transport model driven by assimilated meteorological fields from the Goddard Earth Observing System (GEOS-5) of the NASA Global Modeling and Assimilation Office. The HCN simulation in GEOS-Chem was first described by Li et al. (2003). We use version v8-02-01 of the model, with updates to the HCN simulation based on Li et al. (2009). We employ the meteorological fields at a horizontal resolution of 2×2.5 degrees, degraded from their native resolution of 0.5×0.67 degrees. The model has 47 vertical layers ranging from the surface to 0.01 hPa. Biomass burning emissions, the primary source of HCN, are specified based on monthly mean biomass burning emissions of CO from the Global Fire Emission Database v2 (GFED2), with an assumed HCN/CO emission scale factor of 0.27 % (Li et al., 2003). Monthly mean biofuel emissions of HCN are based on CO emissions from Streets et al. (2003), following Li et al. (2009), with an HCN/CO emission scale factor of 1.6 % (Li et al., 2003). The global annual source of HCN simulated in the model between 2001 and 2008 varied between 0.56 and 0.77 Tg N yr^{-1} (Li et al., 2009). The main sink of HCN is ocean uptake, which is estimated at 0.73 Tg N yr^{-1} (Li et al., 2003). Loss of HCN through reaction with OH in the atmosphere is captured using specified OH fields from a full-chemistry simulation of the model (Li et al., 2009). To remove the influence of the initial conditions on the HCN fields presented here, we spun up the model for two years, between 2002–2003, using an earlier version of the meteorological fields, GEOS-4, that were available for that period.

5.1.2 Organic compounds simulated in IMAGESv2

The IMAGESv2 global chemistry transport model is run at a horizontal resolution of 2×2.5 degrees and is discretized vertically in 40 levels from the surface to the lower

stratosphere. A detailed description of the model can be found in Müller and Brasseur (1995); Müller and Stavrakou (2005); Stavrakou et al. (2009). Here we describe the atmospheric budget of C_2H_6, C_2H_2, CH_3OH and HCOOH as simulated by IMAGESv2.

Fossil fuel and biofuel NMVOC emissions are obtained from the RETRO database (Schultz et al., 2008) for the year 2000 and are overwritten by the REAS inventory over Asia (Ohara et al., 2007) for each corresponding year of simulation. Vegetation fire emissions are obtained from the GFED3 inventory (van der Werf et al., 2010), through application of updated (in 2007) emission factors (Andreae and Merlet, 2001). The large-scale fire emissions are distributed over six layers from the surface to 6 km according to Dentener et al. (2006). Isoprene emissions are obtained from the MEGAN-ECMWF inventory (Müller et al., 2008) and amount to 416, 423, 424 and 437 Tg annually on the global scale, in 2004, 2007, 2009, and 2010, respectively. Meteorological fields are obtained from ECMWF ERA-Interim analyses.

About 70 % of the global source of C_2H_2 and C_2H_6, estimated at about 5 and 10 $Tg\,yr^{-1}$, respectively, is due to anthropogenic activities, the remainder to biomass burning events. The emission factors for tropical forest, extratropical forest and savanna burning emissions are 0.402, 0.260 and 0.269 g of C_2H_2 per kg of dry matter, and 1.202, 0.733, and 0.325 g of C_2H_6 per kg of dry matter, respectively. Both gases are removed from the troposphere through oxidation by OH. In the case of ethane, a small fraction of about 5 % is removed through reaction with chlorine radicals in the lower stratosphere. The global lifetime is calculated at about 2 weeks for C_2H_2 and 2 months for C_2H_6. The impact of changing their biomass burning or anthropogenic emission sources is investigated through sensitivity studies (see Sect. 5.2.2).

Both methanol and formic acid have direct emissions from anthropogenic activities, fires and vegetation, as well as a secondary production source. The methanol source, in the standard simulation with the IMAGESv2 model, is estimated at about 200 $Tg\,yr^{-1}$ globally, and is mostly due to the terrestrial vegetation (54 %), oceans (22 %), and photochemistry (16 %) (Millet et al., 2008; Stavrakou et al., 2011). The global source of formic acid in the standard run amounts to 36 $Tg\,yr^{-1}$, of which two thirds is due to secondary production (Paulot et al., 2011; Stavrakou et al., 2012). The emission factors for tropical forest, extratropical forest and savanna burning per kg of dry matter are, respectively, 1.984, 1.798, and 1.47 g of CH_3OH, and 1.13, 2.43 and 0.63 g of HCOOH. Methanol emitted from vegetation is obtained from the MEGANv2.1 emission model (Stavrakou et al., 2011, http://accent.aero.jussieu.fr/database_table_inventories.php), and direct emissions of formic acid from plant leaves are taken from Lathière et al. (2006). Methanol and formic acid are removed through OH oxidation, and wet and dry deposition, and their global lifetimes are estimated as about 6 and 4 days, respectively.

Table 4. Sources of C_2H_6, C_2H_2, CH_3OH and HCOOH in the Southern Hemisphere in $Tg\,yr^{-1}$, as implemented in the standard simulation of the IMAGES model, for the different categories (Categ.): anthropogenic (Anthr.), biomass burning (BB), biogenic (Biog.), and photochemical (Phot.). The Southern Hemispheric emission ratios (ER), from IMAGESv2, of the species relative to CO are also given in mole/mole.

Species	Categ.	2004	2007	2009	2010	ER
C_2H_6	Anthr.	1.48	1.49	1.50	1.50	
	BB	1.67	1.94	1.15	2.21	0.0085
C_2H_2	Anthr.	0.48	0.48	0.49	0.49	
	BB	0.77	0.86	0.55	0.95	0.0043
	Anthr.	2.8	2.8	2.8	2.8	
CH_3OH	BB	4.0	4.44	2.91	4.86	0.018
	Biog.	66.3	65.9	66.2	67.8	
	Phot.	14.9	15.0	15.3	14.0	
	Anthr.	2.59	2.59	2.59	2.59	
HCOOH	BB	2.00	2.26	1.45	2.49	0.0065
	Phot.	12.8	13.0	12.6	11.9	

Two source inversion studies of CH_3OH and HCOOH emissions have been performed based on the IMAGESv2 model constrained by one complete year of satellite column measurements retrieved from the IASI sounder in 2009 (Razavi et al., 2011; Stavrakou et al., 2011, 2012). The global optimized methanol source totals 187 Tg yr^{-1}, close to the a priori, but large decreases in the biogenic sources were inferred over tropical forests of South America and Indonesia. Both biogenic and pyrogenic emissions were decreased by the inversion over Central and Southern Africa compared to the a priori inventories. Regarding HCOOH, a strong increase is deduced from the inversion using IASI HCOOH column data. It is found that 100–120 Tg of formic acid is produced annually, i.e. two to three times more than estimated from known sources (Stavrakou et al., 2012). The source increase is attributed to biogenic sources, either due to direct emission or to the oxidation of biogenic volatile organic compounds. The biomass burning source inferred from the inversion remains close to the a priori. The results were validated by extensive comparisons with (mostly ground-based) HCOOH concentration measurements. The modeled columns at Reunion Island before and after source inversion are presented in Sect. 5.2.3.

The Southern Hemispheric emissions of the discussed compounds in the different years are given in Table 4. Regarding biomass burning, the average emission ratios of these species with respect to CO in the Southern Hemisphere are also given in the table.

5.2 Comparisons of modeled and observed FTIR columns

We show comparisons between FTIR total columns and model total columns c. Since the FTIR total column

averaging kernels **a** (Fig. 3) are not ideal (= 1 at all altitudes), we degrade the model vertical profile to the FTIR vertical resolution, in order to obtain the model "smoothed" total column c_{smoothed}, which represents what the FTIR would measure if the model profile was the true state. We follow Eq. (25) of Rodgers and Connor (2003):

$$c_{\text{smoothed}} = c_{\text{a}} + \mathbf{a}(\mathbf{pc}_{\text{model}} - \mathbf{pc}_{\text{a}}), \quad (1)$$

$\mathbf{pc}_{\text{model}}$ and $\mathbf{pc}_{\text{a}}$, being respectively the model and the FTIR a priori vertical profiles expressed in partial columns (molec cm^{-2}) and c_{a} the FTIR a priori total column.

5.2.1 Hydrogen cyanide (HCN)

We show in Fig. 4 the FTIR time-series of HCN daily mean total columns measured at Reunion Island, together with, for the years 2004 and 2007, the GEOS-Chem HCN total columns, before and after the smoothing with the FTIR total column averaging kernel (Eq. 1). We do not show, for HCN, the model results for the years 2009 and 2010, because the fire database GFED3 (van der Werf et al., 2010) was not implemented in v8-02-01 of GEOS-Chem and the GFED2 currently used does not provide data after 2008. The standard GEOS-Chem run underestimates the HCN total columns at Reunion Island during September–October. As seen in Sect. 5.1.1, the standard model uses a global HCN/CO emission scale factor of 0.27 % for biomass burning emissions of HCN. As a sensitivity test, a simulation was conducted with a biomass burning emission ratio HCN/CO in the Southern Hemisphere equal to 0.47 %, i.e., the value derived from our FTIR measurements (see Sect. 4). The agreement between the model and the FTIR data is greatly improved, especially when comparing the model output before smoothing it by the FTIR averaging kernels.

The agreement between the model and FTIR data is supposed to be improved by the use of the FTIR averaging kernels, whereas the opposite behaviour is observed here. This can be understood by considering the shape of the HCN total column averaging kernel (Fig. 3), and the shape of the model profile simulated during the biomass burning season given in Fig. 7, which is very different from the FTIR a priori and retrieved profiles. The model profile shows a biomass burning enhancement peak at about 4 km, while the peak is located at 6–7 km in the FTIR data. Due to the low sensitivity of the FTIR retrieval to altitudes below 5 km (Fig. 3), the smoothed model profile in the biomass burning season is strongly reduced below 5 km, and therefore also the total column. However, in May–July, the smoothed model total columns are similar to the direct model total columns, in agreement with the profile shapes shown in Fig. 7. This implies that if an enhancement in HCN does occur below 5 km, our FTIR measurements would underestimate it. The FTIR a priori profile, taken from the model WACCMv5 (Sect. 2.2.2), peaks at a higher altitude, about 5–7 km.

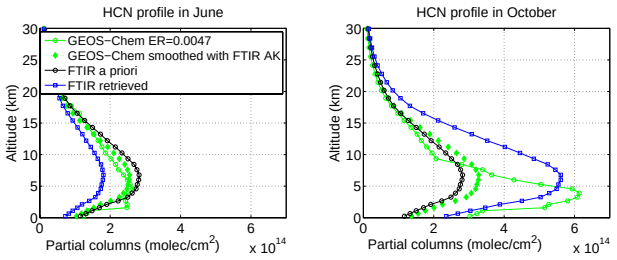

Fig. 7. Example of FTIR and GEOS-Chem HCN profiles (in Partial Columns, molec cm^{-2}) in June and October.

The difference between the WACCM and GEOS-Chem models could reflect differences in the vertical transport in the models. Ott et al. (2009) compared the convective transport in a single column version of the GEOS-5 model with that of a cloud-resolving model and found that GEOS-5 underestimated the convective mass fluxes, which resulted in weaker vertical transport. Liu et al. (2010) showed that, in October 2004 and 2005, upward transport over Southern Africa was weaker in GEOS-5 than in the previous version of the GEOS model, GEOS-4. They also found that convective transport over South America was weaker in GEOS-5 than in GEOS-4 in October 2005.

However, based on the comparisons between the FTIR and the model "smoothed" total columns, the model still underestimates HCN in October, both in 2004 and 2007, suggesting an underestimation of the biomass burning emission inventory (GFED2 in GEOS-Chem) during these months. This seems to be confirmed by the same undersestimation of CO from GEOS-Chem compared to FTIR data (Fig. 4, lower panel).

Table 5 provides mean differences between FTIR and model "smoothed" total columns, mean(FTIR-model)/mean(FTIR), and standard deviations (σ), std(FTIR-model)/mean(FTIR), in percentage, for the different species and the different sensitivity tests, together with the correlation coefficients (R). We see again that for HCN the agreement is significantly improved using a corrected HCN/CO emission ratio of 0.47 %, especially regarding the σ and R values. Despite the positive values of the annual mean differences seen in Table 5, the bias is negative outside the intense biomass burning period (-12 ± 7 % and -22 ± 7 % for the standard and sensitivity runs, respectively), and larger than the systematic error on the FTIR columns (14.5 %) for the sensitivity case, suggesting that the HCN emissions are overestimated in the model during the January–July 2007 period.

5.2.2 Ethane (C_2H_6) and acetylene (C_2H_2)

The modeled time-series of C_2H_6 and C_2H_2 are compared with the FTIR measurements in Fig. 4. The interannual variability of the biomass burning emissions (from GFED3, see

Table 5. Relative (%) mean differences (D) between FTIR and model total columns, mean(FTIR-model)/mean(FTIR), and standard deviations (σ), std(FTIR-model)/mean(FTIR) for the different species and the different sensitivity tests, together with the correlation coefficients R. The model total columns have been smoothed to the FTIR vertical resolution using Eq. (1).

	Annual		Jan–Jul		Aug–Nov	
	$D \pm \sigma$	R	$D \pm \sigma$	R	$D \pm \sigma$	R
HCN						
Standard	20 ± 32	0.77	-12 ± 7	0.20	27 ± 28	0.86
ER = 0.0047	7 ± 26	0.89	-22 ± 7	0.19	12 ± 24	0.89
C_2H_6						
Standard	26 ± 20	0.85	28 ± 15	0.24	23 ± 21	0.80
BB EF doubled	-12 ± 28	0.87	10 ± 15	0.34	-23 ± 22	0.83
Anthr. doubled	-4 ± 22	0.81	-15 ± 16	0.19	-1 ± 22	0.77
C_2H_2						
Standard	35 ± 45	0.62	23 ± 43	0.09	38 ± 40	0.48
BB EF doubled	0 ± 41	0.69	-2 ± 44	0.18	-1 ± 38	0.55
Anthrop. doubled	4 ± 50	0.46	-29 ± 49	0.01	15 ± 43	0.31
CH_3OH						
Standard all years	0 ± 37	0.17	-38 ± 23	0.30	15 ± 32	0.44
Standard 2009	1 ± 31	0.17	-30 ± 20	0.38	17 ± 25	0.70
Optimized 2009	5 ± 26	0.55	-15 ± 20	0.37	19 ± 23	0.64
HCOOH						
Standard all years	58 ± 79	0.64	30 ± 42	0.23	64 ± 66	0.51
Standard 2009	53 ± 79	0.61	20 ± 30	0.16	66 ± 63	0.57
Optimized 2009	-34 ± 57	0.74	-74 ± 46	0.10	-18 ± 52	0.62

Table 4) is reflected by lower model columns of C_2H_6 and C_2H_2 in 2009, and higher columns in 2010.

Doubling the pyrogenic source, by doubling the C_2H_6 and C_2H_2 emission factors, is found to improve the overall agreement with FTIR data, as evidenced by the slightly higher correlation coefficient in this case (Table 5). But, the Southern Hemispheric emission ratio C_2H_6/CO in the standard IMAGESv2 model (0.0085, Table 4) is very close to the FTIR derived value (0.0078), and the C_2H_2 emission ratio is already larger (0.0043) than the FTIR value (0.002), implying that the CO pyrogenic emissions are also underestimated in the GFED3 inventory used in IMAGESv2. This is confirmed by the CO comparisons between IMAGESv2 and FTIR (Fig. 4, bottom panel). Additional considerations confirm that the emission factors are not the cause of the disagreement. First, the standard deviation is higher with doubled emission factors for C_2H_6. This is well explained by examining the time-series of Fig. 4: while the peak in October is well reproduced for C_2H_6 by this sensitivity run, the model overestimates the C_2H_6 columns during August–mid-September, and again in November 2010. The strong underestimation in late September–October of the standard run is also observed in C_2H_2 and CO. Since the lifetime of C_2H_2 is only 12 days in the Tropics, this suggests that very high biomass burning emissions occurred around late September–October that are underestimated in the GFED3 inventory.

Finally, the simulation using doubled anthropogenic emissions of C_2H_6 and C_2H_2 overestimates the observations during the January-July period and leads to a weaker correlation with the data. However, if the underestimation of biomass burning emissions occurs indeed mainly in late September–October, Table 5 and Fig. 4 during January–July suggest an underestimation of anthropogenic emissions, even if it is well below the factor of two that has been simulated.

5.2.3 Methanol (CH_3OH) and formic acid (HCOOH)

The modeled time-series of CH_3OH and HCOOH are shown in Fig. 4. As expected by the lower contribution of biomass burning emissions compared to the biogenic and photochemical sources (Table 4), the interannual variability of methanol and formic acid is smaller than for C_2H_6 and C_2H_2. But still, the modeled values in late September–October are higher (by about 30 % in the case of methanol) in 2010 than in 2009, reflecting the interannual variability of biomass burning emissions. The similar modeled values in 2004 and 2007 are explained by the fact that the more intense biomass burning season in 2007 occurred only in South America, with little impact on the relatively short-lived compounds considered here, while the 2010 year shows enhanced biomass burning emissions also in Southern Africa (van der Werf et al., 2010, and Sect. 3). In contrast to the model, the FTIR data show enhanced values in 2004, not only for C_2H_6 and C_2H_2, but also for CH_3OH and HCOOH. This leads to the conclusion that the underestimation of biomass burning emissions in September–October 2004, occurs more specifically in the Southeastern Africa-Madagascar region. As in the case of C_2H_2 and C_2H_6, the underestimation of the modeled CH_3OH and HCOOH during the fire season can not be due to the emission factors used in the model, since the ratios CH_3OH/CO and HCOOH/CO have slightly larger values in IMAGESv2 (0.018 and 0.0065, respectively) than in the FTIR observations (0.012 and 0.0056, respectively). From Fig. 4, we see that the standard model IMAGESv2 simulates better the CH_3OH and HCOOH columns in October 2010 compared to 2009, as a consequence of the higher emissions in 2010 in Southern Africa and Madagascar. The fact that the observed CH_3OH and HCOOH columns were roughly as high in 2009 as in 2010 suggests that the biomass burning emissions in Southern Africa-Madagascar should be comparable for both years, if indeed biomass burning is responsible for the high columns observed for these two species during the dry season. The possible underestimation of GFED3 emissions in 2009 could unfortunately not be confirmed by comparisons with the other species, because of the lack of FTIR measurements during that period in the required spectral ranges.

The standard model overestimates the observed CH_3OH columns during the January-July period by about 40 %. The optimization of methanol sources using IASI data over the continents inferred a reduction of biogenic emissions

(Stavrakou et al., 2011), leading to some improvement in the modeled seasonal cycle in comparison with FTIR data in 2009, with a reduction of the negative bias observed in the January–July period (Table 5). Still, the IASI-derived emissions appear too low during the fire season. Monthly means comparisons between IASI at Reunion Island and our FTIR data are shown in Fig. 11 of Stavrakou et al. (2011). Considering the large error bars of IASI, the datasets are in agreement, but the amplitude of the seasonal cycle in IASI is lower than in the FTIR data, and the value for October is 15–20 % lower in IASI. The model overestimation between January and July/August is stronger in 2010 than in 2007 and 2009, for unknown reasons. It could be due to an overestimation of biogenic sources, but also possibly to a misrepresentation of the ocean–atmosphere exchanges in the model. The magnitude and even the sign of this exchange is determined by methanol concentrations in ocean water which are not well constrained. This ocean–atmosphere exchange could not be constrained by the inversion using IASI data, because oceanic IASI data were excluded from the inversion, due to large uncertainties (low signal-to-noise ratio, low thermal contrast). Note however that the overestimation of CH_3OH concentrations by the model in the January–July period is at odds with comparisons of IMAGESv2 with aircraft data in the South Tropical Pacific in Mach–April 1999 (PEM-Tropics-B campaign, Stavrakou et al., 2011), which suggested the existence of a significant ocean source at these latitudes.

Concerning formic acid, underestimated pyrogenic and biogenic emissions in the model are likely responsible for the general model underestimation of the FTIR columns. As shown in Fig. 4, the use of continental 2009 IASI column data to constrain the model in a source inversion scheme using IMAGESv2 (Stavrakou et al., 2012) brings the simulated columns closer to the FTIR data during the dry season and increases the correlation (Table 5). This column enhancement is realized primarily through the introduction of a large source due to the photochemical degradation of biogenic NMVOCs. The inversion also increases the biomass burning source in Southeastern Africa, but this appears to have little influence on the simulated HCOOH columns at Reunion Island (Fig. 4: the red solid line shows the inversion results without the biomass burning source). The fact that biomass burning plays only a minor role in the inversion is a consequence of the dominance of biogenic/photochemical sources over the continental Tropics. The inversion is driven by elevated IASI HCOOH columns over widespread areas in Southern Africa, in regions (e.g., Congo/Angola, see Fig. (S2) in Stavrakou et al., 2012) where biomass burning emissions are small in September and October.

During the January–July period, however, the inversion leads to a significant overestimation of HCOOH columns, for reasons yet unclear. It appears possible that the model overestimates the transport, or underestimates the sink of HCOOH from biogenic emission areas to Reunion Island. Model transport is especially sensitive to fire injection heights, boundary layer mixing, deep convection and horizontal advection, which all have significant (but difficult to quantify) uncertainties. It is worth noting that models have in particular difficulties in reproducing the HCOOH vertical profiles in the upper troposphere, where the modeled mixing ratios are often overestimated (Paulot et al., 2011; Stavrakou et al., 2012), with possibly important consequences for long-range transport, since horizontal winds are usually stronger at those higher altitudes. These issues require further investigation.

Note that the apparent model underestimation of the role of biomass burning as the main driver for HCOOH and CH_3OH variability at Reunion Island does not imply that the global impact of biomass burning on the budget of those species is underestimated by the model. In fact, the enhancement ratios obtained within this study confirm previous estimations and lead to global pyrogenic emission estimates of the order of 5 Tg CH_3OH and 3 Tg HCOOH yr^{-1}, to be compared with total source estimates exceeding 100 Tg yr^{-1} for both compounds.

Finally, Paulot et al. (2011) has shown that a good agreement between the HCOOH columns modeled by GEOS-Chem and the FTIR measurements at Reunion Island can be obtained by assuming that the oxidation of organic aerosol generates a diffuse source of formic acid associated with aerosol aging. Since organic aerosols come primarily from biomass burning in the South Hemisphere, this study confirms our finding, based on our very good correlation between HCOOH and CO, that biomass burning is a dominant source of HCOOH at Reunion Island during the August–November period.

6 Conclusions

We have performed FTIR measurements and retrieval analyses of five important biomass burning products (HCN, C_2H_6, C_2H_2, CH_3OH, and HCOOH) at Reunion Island. The time-series obtained during three measurement campaigns allow the determination of both the seasonality and interannual variability of each species. The influence of biomass burning in the total columns of the target species is clearly observed and, in particular, the correlation with the CO FTIR total columns is very high ($R \geq 0.86$) during the peak of the biomass burning season (August–November). From the correlation plots of the target species versus CO, we have derived enhancement ratios, which are in agreement with previous values reported in the literature: we obtain 0.0047, 0.0078, 0.0020, 0.012, and 0.0046 for HCN, C_2H_6, C_2H_2, CH_3OH, and HCOOH, respectively.

The HCN ground-based data have been compared to the chemical transport model GEOS-Chem, while the other species have been compared to the IMAGESv2 model. We show that using our derived HCN/CO ratio of 0.0047, instead of the 0.0027 value used in the standard GEOS-Chem simulations, improves the agreement between GEOS-Chem and FTIR data. The comparisons between the FTIR HCN total columns and the total columns obtained when the model is "smoothed" with the FTIR averaging kernels suggest an underestimation of the biomass burning emissions in the inventory used in the model (GFED2) in October. This seems to be confirmed by the higher underestimation of CO from GEOS-Chem compared to FTIR during October. We have seen also that an underestimation could result from the lower altitude (4 km) of the peak of HCN simulated in GEOS-Chem compared to the one of the a priori profile used for the FTIR retrievals (6–7 km), which comes from the WACCMv5 model. It suggests that the altitude of the biomass burning outflow over Southern Africa may be too low in the GEOS-Chem model. This should be investigated in the future.

The comparisons between IMAGESv2 and FTIR for the long-lived species C_2H_6 and C_2H_2 lead to the conclusion that the biomass burning emission inventory (GFED3) is probably underestimated in the late September–October period for all years of measurements, and particularly in 2004. The comparisons with CH_3OH and HCOOH, having a lifetime of 6 and 4 days, respectively, show that the underestimation in late September–October 2004, occurs more specifically in the Southeastern Africa-Madagascar region. Note that this result confirms also the underestimation of GFED2 emissions, since the emissions in GFED2 are even lower than in GFED3, especially in this region (Fig. 5). The CH_3OH IASI-derived emissions remain too low during the fire season, suggesting that IASI may underestimate CH_3OH in this period in the Southeastern Africa-Madagascar region. The standard model overestimates the observed CH_3OH columns during the January-July period by about 40 %, and still by 15 % after the inversion using IASI data, possibly due to an overestimation of biogenic sources and/or a misrepresentation of the ocean-atmosphere exchanges in the model.

Although the IMAGESv2 optimization of HCOOH sources using IASI data greatly improves the agreement with FTIR data during the fire season, the model strongly overestimates HCOOH during the January–July period after inversion. However, this better agreement is achieved with only a minor contribution from biomass burning, the dominant one being the introduction of a large source due to the photochemical degradation of biogenic NMVOCs. This specific result at Reunion Island is not in agreement with our finding, based on our very good correlation between HCOOH and CO, that biomass burning is a dominant source of HCOOH at Reunion Island during the August–November period. However, our finding is consistent with the study of Paulot et al. (2011), who have shown that a good agreement between the HCOOH columns modeled by GEOS-Chem and the FTIR measurements at Reunion Island can be achieved by assuming that organic aerosol oxidation generates a diffuse source of formic acid.

We have demonstrated that Reunion Island, close to Africa and Madagascar, is very well located to assess the ability of the chemical transport models to reproduce the biogenic and biomass burning emissions of various species and to evaluate model input parameters such as emission factors and biomass burning emission inventories.

Acknowledgements. This study has been supported by the ESA PRODEX project A3C, as well as the BIOSOA and AGACC-II projects within the "Science for a Sustainable Development" research program funded by the Belgian Science Policy Office. One of the co-authors (G. V.) was funded by the EU Integrated project GEOMON. Work at the University of Toronto was supported by the Natural Sciences and Engineering Research Council of Canada.

Edited by: G. Stiller

References

Akagi, S. K., Yokelson, R. J., Wiedinmyer, C., Alvarado, M. J., Reid, J. S., Karl, T., Crounse, J. D., and Wennberg, P. O.: Emission factors for open and domestic biomass burning for use in atmospheric models, Atmos. Chem. Phys., 11, 4039–4072, doi:10.5194/acp-11-4039-2011, 2011.

Andreae, M. O. and Merlet, P.: Emission of trace gases and aerosols from biomass burning, Global Biogeochem. Cy., 15, 955–966, 2001.

Coheur, P.-F., Clarisse, L., Turquety, S., Hurtmans, D., and Clerbaux, C.: IASI measurements of reactive trace species in biomass burning plumes, Atmos. Chem. Phys., 9, 5655–5667, doi:10.5194/acp-9-5655-2009, 2009.

Cooke, W. F., Koffi, B., and Grégoire, J. M.: Seasonality of vegetation fires in Africa from remote sensing data and application to a global chemistry model, J. Geophys. Res., 101, 21051–21065, doi:10.1029/96JD01835, 1996.

Crutzen, P. J. and Andreae, M. O.: Biomass burning in the tropics: impact on atmospheric chemistry and biogeochemical cycles, Science, 250, 1669–1678, 1990.

Dentener, F., Kinne, S., Bond, T., Boucher, O., Cofala, J., Generoso, S., Ginoux, P., Gong, S., Hoelzemann, J. J., Ito, A., Marelli, L., Penner, J. E., Putaud, J.-P., Textor, C., Schulz, M., van der Werf, G. R., and Wilson, J.: Emissions of primary aerosol and precursor gases in the years 2000 and 1750 prescribed data-sets for AeroCom, Atmos. Chem. Phys., 6, 4321–4344, doi:10.5194/acp-6-4321-2006, 2006.

Duflot, V., Dils, B., Baray, J.-L., De Mazière, M., Attié, J.-L., Vanhaelewyn, G., Senten, C., Vigouroux, C., Clain, G., and Delmas, R.: Analysis of the origin of the distribution of CO in the subtropical Southern Indian Ocean in 2007, J. Geophys. Res., 115, D22106, doi:10.1029/2010JD013994, 2010.

Dufour, G., Boone, C. D., Rinsland, C. P., and Bernath, P. F.: First space-borne measurements of methanol inside aged southern tropical to mid-latitude biomass burning plumes using

the ACE-FTS instrument, Atmos. Chem. Phys., 6, 3463–3470, doi:10.5194/acp-6-3463-2006, 2006.

Duncan, B. N., Martin, R. V., Staudt, A. C., Yevich, R., and Logan, J. A.: Interannual and seasonal variability of biomass burning emissions constrained by satellite observations, J. Geophys. Res., 108, 4100, doi:10.1029/2002JD002378, 2003.

Emmons, L. K., Hauglustaine, D. A., Müller, J.-F., Carroll, M. A., Brasseur, G. P., Brunner, D., Staehelin, J., Thouret, V., Marenco, A.: Data composites of airborne observations of tropospheric ozone and its precursors, J. Geophys. Res., 105, 20497–20538, 2000.

Ferek, R. J., Reid, J. S., Hobbs, P. V., Blake, D. R., and Liousse, C.: Emission factors of hydrocarbons, halocarbons, trace gases and particles from biomass burning in Brazil, J. Geophys. Res., 103, 32107–32118, doi:10.1029/98JD00692, 1998.

González Abad, G., Bernath, P. F., Boone, C. D., McLeod, S. D., Manney, G. L., and Toon, G. C.: Global distribution of upper tropospheric formic acid from the ACE-FTS, Atmos. Chem. Phys., 9, 8039–8047, doi:10.5194/acp-9-8039-2009, 2009.

Harrison, J. J., Allen, N. D. C., and Bernath, P. F.: Infrared absorption cross sections for ethane (C_2H_6) in the 3 µm region, J. Quant. Spectros. Radiat. Transfer, 111, 357–363, 2010.

Hase, F., Blumenstock, T., and Paton-Walsh, C.: Analysis of the instrumental line shape of high-resolution Fourier transform IR spectrometers with gas cell measurements and new retrieval software, Appl. Opt., 38, 3417–3422, 1999.

Hase, F., Demoulin, P., Sauval, A. J., Toon, G. C., Bernath, P. F., Goldman, A., Hannigan, J. W., and Rinsland, C. P.: An empirical line-by-line model for the infrared solar transmittance spectrum from 700 to 5000 cm^{-1}, J. Quant. Spectros. Radiat. Transfer, 102, 450–463, 2006.

Hase, F., Wallace, L., McLeod, S. D., Harrison, J. J., and Bernath, P. F.: The ACE-FTS atlas of the infrared solar spectrum, J. Quant. Spectros. Radiat. Transfer, 111, 521–528, 2010.

Hoell, J. M., Davis, D. D., Jacob, D. J., Rodgers, O., Newell, R. E., Fuelberg, H. E., McNeal, R. J., Raper, J. L., and Bendura, R. J.: Pacific Exploratory Mission in the Tropical Pacific: PEM-Tropics A, August–September 1996, J. Geophys. Res., 104, 5567–5583, doi:10.1029/1998JD100074, 1999.

Hornbrook, R. S., Blake, D. R., Diskin, G. S., Fried, A., Fuelberg, H. E., Meinardi, S., Mikoviny, T., Richter, D., Sachse, G. W., Vay, S. A., Walega, J., Weibring, P., Weinheimer, A. J., Wiedinmyer, C., Wisthaler, A., Hills, A., Riemer, D. D., and Apel, E. C.: Observations of nonmethane organic compounds during ARCTAS – Part 1: Biomass burning emissions and plume enhancements, Atmos. Chem. Phys., 11, 11103–11130, doi:10.5194/acp-11-11103-2011, 2011.

Jacob, D. J., Field, B. D., Li, Q., Blake, D. R., de Gouw, J., Warneke, C. Hansel, A., Wisthaler, A., Singh, H. B., and Guenther, A.: Global budget of methanol: constraints from atmospheric observations, J. Geophys. Res., 110, D08303, doi:10.1029/2004JD005172, 2005.

Lathière, J., Hauglustaine, D. A., Friend, A. D., De Noblet-Ducoudré, N., Viovy, N., and Folberth, G. A.: Impact of climate variability and land use changes on global biogenic volatile organic compound emissions, Atmos. Chem. Phys., 6, 2129–2146, doi:10.5194/acp-6-2129-2006, 2006.

Li, Q., Jacob, D. J., Yantosca, R. M., Heald, C. L., Singh, H. B., Koike, M., Zhao, Y., Sachse, G. W., and Streets, D. G.: A global three-dimensional model analysis of the atmospheric budgets of HCN and CH_3CN: constraints from aircraft and ground measurements, J. Geophys. Res., 108, 8827, doi:10.1029/2002JD003075, 2003.

Li, Q., Palmer, P. I., Pumphrey, H. C., Bernath, P., and Mahieu, E.: What drives the observed variability of HCN in the troposphere and lower stratosphere?, Atmos. Chem. Phys., 9, 8531–8543, doi:10.5194/acp-9-8531-2009, 2009.

Liu, J., Logan, J. A., Jones, D. B. A., Livesey, N. J., Megretskaia, I., Carouge, C., and Nedelec, P.: Analysis of CO in the tropical troposphere using Aura satellite data and the GEOS-Chem model: insights into transport characteristics of the GEOS meteorological products, Atmos. Chem. Phys., 10, 12207–12232, doi:10.5194/acp-10-12207-2010, 2010.

Mahieu, E., Zander, R., Delbouille, L., Demoulin, P., Roland, G., and Servais, C.: Observed trends in total vertical column abundances of atmospheric gases from IR solar spectra recorded at the Jungfraujoch, J. Atmos. Chem., 28, 227–243, 1997.

Meier, A., Toon, G. C., Rinsland, C. P., Goldman, A., and Hase, F.: Spectroscopic Atlas of Atmospheric Microwindows in the Middle Infra-Red, 2nd revised edition, IRF Technical Report 048, ISSN 0284-1738, IRF Institutet för Rymdfysik, Kiruna, Sweden, 2004.

Millet, D. B., Jacob, D. J., Custer, T. G., de Gouw, J. A., Goldstein, A. H., Karl, T., Singh, H. B., Sive, B. C., Talbot, R. W., Warneke, C., and Williams, J.: New constraints on terrestrial and oceanic sources of atmospheric methanol, Atmos. Chem. Phys., 8, 6887–6905, doi:10.5194/acp-8-6887-2008, 2008.

Müller, J.-F. and Brasseur, G.: A three-dimensional chemical transport model of the global troposphere, J. Geophys. Res., 100, 16445–16490, 1995.

Müller, J.-F. and Stavrakou, T.: Inversion of CO and NO_x emissions using the adjoint of the IMAGES model, Atmos. Chem. Phys., 5, 1157–1186, doi:10.5194/acp-5-1157-2005, 2005.

Müller, J.-F., Stavrakou, T., Wallens, S., De Smedt, I., Van Roozendael, M., Potosnak, M. J., Rinne, J., Munger, B., Goldstein, A., and Guenther, A. B.: Global isoprene emissions estimated using MEGAN, ECMWF analyses and a detailed canopy environment model, Atmos. Chem. Phys., 8, 1329–1341, doi:10.5194/acp-8-1329-2008, 2008.

Neefs, E., De Mazière, M., Scolas, F., Hermans, C., and Hawat, T.: BARCOS, an automation and remote control system for atmospheric observations with a Bruker interferometer, Rev. Sci. Instrum., 78, 035109-1–0035109-9, 2007.

Notholt, J., Toon, G. C., Lehmann, R., Sen, B., and Blavier, J.-F.: Comparison of Arctic and Antarctic trace gas column abundances from groud-based Fourier transform infrared spectrometry, J. Geophys. Res., 102, 12863–12869, 1997.

Notholt, J., Toon, G. C., Rinsland, C. P., Pougatchev, N. S., Jones, N. B., Connor, B. J., Weller, R., Gautrois, M., and Schrems, O.: Latitudinal variations of trace gas concentrations measured by solar absorption spectroscopy during a ship cruise, J. Geophys. Res., 105, 1337–1349, 2000.

Ohara, T., Akimoto, H., Kurokawa, J., Horii, N., Yamaji, K., Yan, X., and Hayasaka, T.: An Asian emission inventory of anthropogenic emission sources for the period 1980–2020, Atmos. Chem. Phys., 7, 4419–4444, doi:10.5194/acp-7-4419-2007, 2007.

Ott, L. E., Bacmeister, J., Pawson, S., Pickering, K., Stenchikov, G., Suarez, M., Huntrieser, H., Loewenstein, M., Lopez, J., and Xueref-Remy, I.: Analysis of Convective Transport and Parameter Sensitivity in a Single Column Version of the Goddard Earth Observation System, Version 5, General Circulation Model, J. Atmos. Sci., 66, 627–646, 2009.

Paton-Walsh, C., Wilson, S. R., Jones, N. B., and Griffith, D. W. T.: Measurement of methanol emissions from Australian wildfires by ground-based solar Fourier transform spectroscopy, Geophys. Res. Lett., 35, L08810, doi:10.1029/2007GL032951, 2008.

Paton-Walsh, C., Deutscher, N. M., Griffith, D. W. T., Forgan, B. W., Wilson, S. R., Jones, N. B., and Edwards, D. P.: Trace gas emissions from savanna fires in Northern Australia, J. Geophys. Res., 115, D16314, doi:10.1029/2009JD013309, 2010.

Paulot, F., Wunch, D., Crounse, J. D., Toon, G. C., Millet, D. B., DeCarlo, P. F., Vigouroux, C., Deutscher, N. M., González Abad, G., Notholt, J., Warneke, T., Hannigan, J. W., Warneke, C., de Gouw, J. A., Dunlea, E. J., De Mazière, M., Griffith, D. W. T., Bernath, P., Jimenez, J. L., and Wennberg, P. O.: Importance of secondary sources in the atmospheric budgets of formic and acetic acids, Atmos. Chem. Phys., 11, 1989–2013, doi:10.5194/acp-11-1989-2011, 2011.

Randriambelo, T., Baldy, S., Bessafi, M. Petit, M., and Despinoy, M.: An improved detection and characterization of active fires and smoke plumes in Southeastern Africa and Madagascar, Int. J. Remote Sensing, 19, 2623–2638, 1998.

Randriambelo, T., Baray, J.-L., and Baldy, S.: Effect of biomass burning, convective venting, and transport on tropospheric ozone over the Indian Ocean: Reunion Island field observations, J. Geophys. Res., 105, 11813–11832, doi:10.1029/1999JD901097, 2000.

Raper, J., Kleb, M., Jacob, D., Davis, D., Newell, R., Fuelberg, H., Bendura, R., Hoell, J., and McNeal, R.: Pacific Exploratory Mission in the Tropical Pacific: PEM-Tropics B, March–April 1999, J. Geophys. Res., 106, 32401–32425, 2001.

Razavi, A., Karagulian, F., Clarisse, L., Hurtmans, D., Coheur, P. F., Clerbaux, C., Müller, J. F., and Stavrakou, T.: Global distributions of methanol and formic acid retrieved for the first time from the IASI/MetOp thermal infrared sounder, Atmos. Chem. Phys., 11, 857–872, doi:10.5194/acp-11-857-2011, 2011.

Rinsland, C. P., Jones, N. B., Connor, B. J., Logan, J. A., Pougatchev, N. S., Goldman, A., Murcray, F. J., Stephen, T. M., Pine, A. S., Zander, R., Mahieu, E., and Demoulin, P.: Northern and Southern Hemisphere ground-based infrared spectroscopic measurements of tropospheric carbon monoxide and ethane, J. Geophys. Res., 103, 28197–28217, 1998.

Rinsland, C. P., Goldman, A., Murcray, F. J., Stephen, T. M., Pougatchev, N. S., Fishman, J., David, S. J., Blatherwick, R. D., Novelli, P. C., Jones, N. B., and Connor, B. J.: Infrared solar spectroscopic measurements of free tropospheric CO, C_2H_6, and HCN above Mauna Loa, Hawaii: seasonal variations and evidence for enhanced emissions from the Southeast Asian tropical fires of 1997–1998, J. Geophys. Res., 104, 18667–18680, doi:10.1029/1999JD900366, 1999.

Rinsland, C. P., Meier, A., Griffith, D. W. T., and Chiou, L. S.: Ground-based measurements of tropospheric CO, C_2H_6, and HCN from Australia at 34° S latitude during 1997–1998, J. Geophys. Res., 106, 20913–20924, doi:10.1029/2000JD000318, 2001.

Rinsland, C. P., Jones, N. B., Connor, B. J., Wood, S. W., Goldman, A., Stephen, T. M., Murcray, F. J., Chiou, L. S., Zander, R., and Mahieu, E.: Multiyear infrared solar spectroscopic measurements of HCN, CO, C_2H_6, and C_2H_2 tropospheric columns above Lauder, New Zealand (45° S latitude), J. Geophys. Res., 107, 4185, doi:10.1029/2001JD001150, 2002.

Rinsland, C. P., Mahieu, E., Zander, R., Goldman, A., Wood, S., and Chiou, L.: Free tropospheric measurements of formic acid (HCOOH) from infrared ground-based solar absorption spectra: retrieval approach, evidence for a seasonal cycle, and comparison with model calculations, J. Geophys. Res., 109, D18308, doi:10.1029/2004JD004917, 2004.

Rinsland, C. P., Boone, C. D., Bernath, P. F., Mahieu, E., Zander, R., Dufour, G., Clerbaux, C., Turquety, S., Chiou, L., McConnell, J. C., Neary, L., and Kaminski, J. W.: First space-based observations of formic acid (HCOOH): Atmospheric Chemistry Experiment austral spring 2004 and 2005 Southern Hemisphere tropical-mid-latitude upper tropospheric measurements, Geophys. Res. Lett., 33, L23804, doi:10.1029/2006GL027128, 2006.

Rinsland, C. P., Dufour, G., Boone, C. D. , Bernath, P. F. , Chiou, L., Coheur, P. F., Turquety, S., and Clerbaux, C.: Satellite boreal measurements over Alaska and Canada during June–July 2004: Simultaneous measurements of upper tropospheric CO, C_2H_6, HCN, CH_3Cl, CH_4, C_2H_2, CH_3OH, HCOOH, OCS, and SF_6 mixing ratios, Global Biogeochem. Cy., 21, GB3008, doi:10.1029/2006GB002795, 2007.

Rinsland, C. P., Mahieu, E., Chiou, L., and Herbin, H.: First ground-based infrared solar absorption measurements of free tropospheric methanol (CH_3OH): multidecade infrared time series from Kitt Peak (31.9° N 111.6° W): trend, seasonal cycle, and comparison with previous measurements, J. Geophys. Res., 114, D04309, doi:10.1029/2008JD011003, 2009.

Rodgers, C. D.: Inverse Methods for Atmospheric Sounding: Theory and Practice, Series on Atmospheric, Oceanic and Planetary Physics – Vol. 2, World Scientific Publishing Co., Singapore, 2000.

Rodgers, C. D. and Connor, B. J.: Intercomparison of remote sounding instruments, J. Geophys. Res., 108, 4116–4129, 2003.

Rothman, L. S., Gordon, I. E., Barbe, A., Benner, D. C., Bernath, P. F., Birk, M., Boudon, V., Brown, L. R., Campargue, A., Champion, J.-P., Chance, K., Coudert, L. H., Danaj, V., Devi, V. M., Fally, S., Flaud, J.-M., Gamache, R. R., Goldmanm, A., Jacquemart, D., Kleiner, I., Lacome, N., Lafferty, W. J., Mandin, J.-Y., Massie, S. T., Mikhailenko, S. N., Miller, C. E., Moazzen-Ahmadi, N., Naumenko, O. V., Nikitin, A. V., Orphal, J., Perevalov, V. I., Perrin, A., Predoi-Cross, A., Rinsland, C. P., Rotger, M., Šimečková, M., Smith, M. A. H., Sung, K., Tashkun, S. A., Tennyson, J., Toth, R. A., Vandaele, A. C., and Vander Auwera, J.: The Hitran 2008 molecular spectroscopic database, J. Quant. Spectrosc. Radiat. Transfer, 110, 533–572, 2009.

Schultz, M. G., Heil, A., Hoelzemann, J. J., Spessa, A., Thonicke, K., Goldammer, J. G., Held, A. C., Pereira, J. M. C., and van het Bolscher, M.: Global wildland fire emissions from 1960 to 2000, Global Biogeochem. Cy., 22, GB2002, doi:10.1029/2007GB003031, 2008.

Senten, C., De Mazière, M., Dils, B., Hermans, C., Kruglanski, M., Neefs, E., Scolas, F., Vandaele, A. C., Vanhaelewyn, G.,

Vigouroux, C., Carleer, M., Coheur, P. F., Fally, S., Barret, B., Baray, J. L., Delmas, R., Leveau, J., Metzger, J. M., Mahieu, E., Boone, C., Walker, K. A., Bernath, P. F., and Strong, K.: Technical Note: New ground-based FTIR measurements at Ile de La Réunion: observations, error analysis, and comparisons with independent data, Atmos. Chem. Phys., 8, 3483–3508, doi:10.5194/acp-8-3483-2008, 2008.

Sinha, P., Hobbs, P. V., Yokelson, R. J., Bertschi, I. T., Blake, D. R., Simpson, I. J., Gao, S., Kirchstetter, T. W., and Novakov, T.: Emissions of trace gases and particles from savanna fires in Southern Africa, J. Geophys. Res., 108, 8487, doi:10.1029/2002JD002325, 2003.

Sivakumar, V., Baray, J.-L., Baldy, S., and Bencherif, H.: Tropopause characteristics over a southern subtropical site, Reunion Island (21° S, 55° E): using radiosonde-ozonesonde data, J. Geophys. Res., 111, D19111, doi:10.1029/2005JD006430, 2006.

Stavrakou, T., Müller, J.-F., De Smedt, I., Van Roozendael, M., van der Werf, G. R., Giglio, L., and Guenther, A.: Evaluating the performance of pyrogenic and biogenic emission inventories against one decade of space-based formaldehyde columns, Atmos. Chem. Phys., 9, 1037–1060, doi:10.5194/acp-9-1037-2009, 2009.

Stavrakou, T., Guenther, A., Razavi, A., Clarisse, L., Clerbaux, C., Coheur, P.-F., Hurtmans, D., Karagulian, F., De Mazière, M., Vigouroux, C., Amelynck, C., Schoon, N., Laffineur, Q., Heinesch, B., Aubinet, M., Rinsland, C., and Müller, J.-F.: First space-based derivation of the global atmospheric methanol emission fluxes, Atmos. Chem. Phys., 11, 4873–4898, doi:10.5194/acp-11-4873-2011, 2011.

Stavrakou, T., Müller, J.-F., Peeters, J., Razavi, A., Clarisse, L., Clerbaux, C., Coheur, P.-F., Hurtmans, D., De Mazière, M., Vigouroux, C., Deutscher, N. M., Griffith, D. W. T., Jones, N., and Paton-Walsh, C.: Satellite evidence for a large source of formic acid from boreal and tropical forests, Nature Geosci., 5, 26–30, doi:10.1038/ngeo1354, 2012.

Steck, T.: Methods for determining regularization for atmospheric retrieval problems, Appl. Opt., 41, 1788–1797, 2002.

Streets, D. G., Bond, T. C., Carmichael, G. R., Fernandes, S. D., Fu, Q., He, D., Klimont, Z., Nelson, S. M., Tsai, N. Y., Wang, M. Q., Woo, J.-H., Yarber, K. F.: An inventory of gaseous and primary aerosol emissions in Asia in the year 2000, J. Geophys. Res., 108, 8809, doi:10.1029/2002JD003093, 2003.

Tereszchuk, K. A., González Abad, G., Clerbaux, C., Hurtmans, D., Coheur, P.-F., and Bernath, P. F.: ACE-FTS measurements of trace species in the characterization of biomass burning plumes, Atmos. Chem. Phys., 11, 12169–12179, doi:10.5194/acp-11-12169-2011, 2011.

Tikhonov, A.: On the solution of incorrectly stated problems and a method of regularization, Dokl. Acad. Nauk SSSR, 151, 501–504, 1963.

Vigouroux, C., De Mazière, M., Demoulin, P., Servais, C., Hase, F., Blumenstock, T., Kramer, I., Schneider, M., Mellqvist, J., Strandberg, A., Velazco, V., Notholt, J., Sussmann, R., Stremme, W., Rockmann, A., Gardiner, T., Coleman, M., and Woods, P.: Evaluation of tropospheric and stratospheric ozone trends over Western Europe from ground-based FTIR network observations, Atmos. Chem. Phys., 8, 6865–6886, doi:10.5194/acp-8-6865-2008, 2008.

Vigouroux, C., Hendrick, F., Stavrakou, T., Dils, B., De Smedt, I., Hermans, C., Merlaud, A., Scolas, F., Senten, C., Vanhaelewyn, G., Fally, S., Carleer, M., Metzger, J.-M., Müller, J.-F., Van Roozendael, M., and De Mazière, M.: Ground-based FTIR and MAX-DOAS observations of formaldehyde at Réunion Island and comparisons with satellite and model data, Atmos. Chem. Phys., 9, 9523–9544, doi:10.5194/acp-9-9523-2009, 2009.

van der Werf, G. R., Randerson, J. T., Giglio, L., Collatz, G. J., Mu, M., Kasibhatla, P. S., Morton, D. C., DeFries, R. S., Jin, Y., and van Leeuwen, T. T.: Global fire emissions and the contribution of deforestation, savanna, forest, agricultural, and peat fires (1997–2009), Atmos. Chem. Phys., 10, 11707–11735, doi:10.5194/acp-10-11707-2010, 2010.

Xiao, Y., Jacob, D. J., and Turquety, S.: Atmospheric acetylene and its relationship with CO as an indicator of air mass age, J. Geophys. Res., 112, D12305, doi:10.1029/2006JD008268, 2007.

Xiao, Y., Logan, J. A., Jacob, D. J., Hudman, R. C., Yantosca, R., and Blake, D. R.: Global budget of ethane and regional constraints on US sources, J. Geophys. Res., 113, D21306, doi:10.1029/2007JD009415, 2008.

Zander, R., Duchatelet, P., Mahieu, E., Demoulin, P., Roland, G., Servais, C., Auwera, J. V., Perrin, A., Rinsland, C. P., and Crutzen, P. J.: Formic acid above the Jungfraujoch during 1985–2007: observed variability, seasonality, but no long-term background evolution, Atmos. Chem. Phys., 10, 10047–10065, doi:10.5194/acp-10-10047-2010, 2010.

Zhao, Y., Strong, K., Kondo, Y., Koike, M., Matsumi, Y., Irie, H., Rinsland, C. P., Jones, N. B., Suzuki, K., Nakajima, H., Nakane, H., and Murata, I: Spectroscopic measurements of tropospheric CO, C_2H_6, C_2H_2, and HCN in Northern Japan, J. Geophys. Res., 107, 4343, doi:10.1029/2001JD000748, 2002.